Developing an Appropriate 3D Phenotyping Framework and Establishing Fractal Dimension as Complexity Indicator for Soybean Root System Architecture

Prabhjot Singh Sanghera

Department of Plant Science

Faculty of Agricultural and Environmental Sciences

McGill University

Montreal, Quebec, Canada

August 2024

A thesis submitted to McGill University in partial fulfilment of the requirements of the degree of Master of Science

© Prabhjot Singh Sanghera, 2024

Table of Contents

List of Tables

List of Figures

List of Appendices

Abstract

The development and yield of soybean (*Glycine max*) depend heavily on root system architecture (RSA), which is a key element for water and nutrient uptake. Traditional methods for studying RSA often rely on destructive sampling techniques, such as “shovelomics”, which hinder continuous observation and analysis. Spatial changes in RSA cannot be quantified with traditional 2D methods or 3D methods using artificial growing media, as these methods often fail to capture the spatial distribution of roots in their natural environment. In this master's thesis, an innovative framework is presented for non-destructive 3D phenotyping, using computed tomography (CT) combined with fractal dimension (FD) estimation, to more accurately capture and characterise the complexity of root systems in a sieved sandy soil. In a preliminary step, a classification analysis of 137 soybean cultivars was performed based on RSA trait measurements (excluding FD) made in a previous 2D study. This classification led to the selection of a representative subset of 30 cultivars for a 3D study and in-depth analysis in a subsequent step. Our results support that FD is a key parameter for understanding RSA in 3D. In particular, 37.9% of the observed variation for this trait is accounted for by differences among cultivars (p-value = 0.0192), with the remaining 62.1% attributed to variation among replicate plants of the same cultivar and the experimental error. The transition from 2D to 3D phenotyping has significantly improved the underground perspective of the spatial distribution of soybean roots at an early stage of development in a natural environment, and FD replaced and integrated multiple RSA traits based on angles and root lengths. It now remains to extend the CT-FD combination to larger spatial and temporal scales, to identify cultivars with improved resilience and increased efficiency in varied and challenging environmental conditions. This advanced 3D phenotyping approach appears essential for the development of robust soybean cultivars, thus contributing to sustainable agriculture and food security.

Résumé

Le développement et le rendement du soja (*Glycine max*) dépendent fortement de l'architecture du système racinaire (ASR), qui est un élément clé pour l'absorption de l'eau et des nutriments. Les méthodes traditionnelles d'étude de l'ASR reposent souvent sur des techniques d'échantillonnage destructives, telles que le "shovelomics", qui entravent l'observation et l'analyse en continu. Les changements spatiaux dans l'ASR ne peuvent pas être quantifiés avec les méthodes traditionnelles en 2D, ni avec les méthodes 3D utilisant des milieux de croissance artificiels, car ces méthodes ne parviennent pas la plupart du temps à capturer la distribution spatiale des racines dans leur environnement naturel. Dans ce mémoire de maîtrise, un cadre novateur est présenté pour le phénotypage 3D non-destructif, utilisant la tomodensitométrie assistée par ordinateur (TAO) combinée à l'estimation de la dimension fractale (DF), afin de capturer et de caractériser plus précisément la complexité des systèmes racinaires dans un sol sablonneux tamisé. Dans une étape préliminaire, une analyse de classification de 137 cultivars de soja a été réalisée sur base de mesures de traits ASR (n'incluant pas la DF) prises dans une étude 2D antérieure. Cette classification a conduit à la sélection d'un sous-ensemble représentatif de 30 cultivars pour une étude 3D et une analyse approfondie dans une étape subséquente. Nos résultats montrent que la DF est un paramètre primordial pour comprendre l'ASR en 3D. En particulier, 37,9 % de la variation de ce trait est prise en compte par les différences entre cultivars (p-value = 0,0192), les 62,1% résiduels étant pour la variation entre plants-réplicats d'un même cultivar et l'erreur expérimentale. Le passage du phénotypage 2D au phénotypage 3D a considérablement amélioré la perspective souterraine de la distribution spatiale des racines d'un plant de soja en début de développement dans un milieu naturel, et la DF a remplacé en les intégrant plusieurs traits ASR basés sur des angles et des longueurs de racines. Il reste maintenant à étendre la combination TAO-DF à de plus grandes échelles spatiale et temporelle, afin d'identifier des cultivars à la résilience améliorée et à une efficacité

accrue dans des conditions environnementales variées, voire extrêmes. Cette approche avancée de phénotypage 3D apparaît essentielle pour le développement de cultivars de soja robustes, contribuant à une agriculture durable et à la sécurité alimentaire.

Acknowledgements

This thesis would not have been possible without the guidance and help of several individuals who contributed to its preparation and completion. I express my deepest gratitude to my supervisor, Dr. Pierre R.L. Dutilleul, for his guidance, patience, support, and encouragement, which enabled me to complete my Master's within the available time frame as an international student. His 'One step, one day at a time' approach has positively influenced my outlook on life. I am grateful to FRQNT for its financial support (Subvention Projet en équipe, F. Belzile and P. Dutilleul) and to CFI for making a modern CT scanner available for my research work, through the Geitmann CFI 9 grant and the ECP3 platform.

I thank Dr. Donald L. Smith for his insights during committee meetings, Erin Minnet for helping me settle smoothly, and Dr. Jean-Benoit Charron for his support. I am grateful to Dr. François Belzile for his invaluable advice and encouragement. Thanks also to Mr. Liwen Han for assisting with CT scanning and root image analysis, and Miss Mounawarath Assani for her technical help at the project's initial stages.

A select group of people have made living in Sainte-Anne-de-Bellevue and attending University a pleasure. A big thank you to Severus, Braiden, Isabelle, Diksha, and Preet. Special thanks to Meha and Diljot for the unforgettable parties and their joyous company at the Macdonald Campus. Despite being in different parts of the world, my best friends Lakshay Sharma, Lakshya, and Gurleen have consistently brought smiles to my face throughout my undergraduate and graduate years. I couldn't ask for better friends.

Without the support of a few special people, completing an international Master's degree would have seemed unattainable. My brother has endured my crankiness, rants, and panic with assuring words, smiles, and sometimes memes. The most significant acknowledgement is reserved for my parents. Their love and support have enabled me to achieve everything I set my mind to. I dedicate this thesis to my ama and appa with immense gratitude.

Preface and Contribution of Authors

This thesis consists of five chapters, preceded by a general introduction (Chapter 1) that demonstrates the overall objective. Chapter two is the literature review that describes the importance of root system architecture and innovative phenotyping methodologies that can contribute to the development of soybean cultivars with optimised root systems, and concludes by proposing future work needed to quantify and understand the complexity of the root system architecture. Chapter three proposes a concept of clustering the soybean cultivars into a subset of 30 clusters from larger data using statistical tools. Then, I apply the non-invasive imaging techniques and fractal analysis in chapter four to gain insight into the root system complexity and architecture in the sand. Chapters 3 and 4 are written in manuscript format according to the guidelines of the Graduate and Postdoctoral Studies Office, McGill University. Connecting paragraphs between these chapters are used to explain the logical flow and progression from one manuscript to the next.

The candidate was the first author of all manuscripts, co-authored by Dr. Pierre R.L. Dutilleul. The candidate wrote the literature review and was responsible for experimental design, data collection, data analysis, result interpretation and manuscript writing. Dr. Pierre R.L. Dutilleul provided advice about concept establishment, image analysis, experimental design and processing, data analysis and manuscript revision. This project was funded by Fonds de recherche du Québec – Nature et Technologies (FRQNT).

The manuscript-based chapters are presented in the following order:

Chapter 3. Sanghera, Prabhjot, François Belzile, Waldiodio Seck and Pierre Dutilleul. “Cluster Analysis of 137 Soybean Lines Based on Root System Architecture Traits Measured in Rhizoboxes.” J Biom Biosta 14 (2023): 179.**DOI:** 10.37421/2155-6180.2023.14.179

Chapter 4. Prabhjot Sanghera, Liwen Han, Donald L. Smith, François Belzile, and Pierre Dutilleul. “Developing an Appropriate 3D Phenotyping Framework and Establishing Fractal Dimension as Complexity Indicator for Soybean Root System Architecture” (In preparation for a peer-reviewed journal).

Chapter 1: Introduction

General Introduction

In a world where sustainable agriculture intersects with the quest for nutritional security for both humans and animals, the soybean emerges as a protagonist in an unfolding narrative of innovation, resilience, and global impact. Soybean (*Glycine max*) is a legume widely grown around the world. It is known as the "golden bean" or "miracle bean" because it is a viable source of human nutrition and bioenergy in the twenty-first century (Islam et al., 2019; Singh et al., 2018). Originally from Asia, soybeans are now grown worldwide. This rapid expansion has led to new uses for soybeans in daily life, as they are considered the most acceptable plant protein source in the form of food products such as edamame, tofu, and soy milk. Soybeans yield more oil and protein seeds than wheat, rice, and maize. Soybeans constitute 35% protein, 25-30% carbs, and a variety of polyunsaturated fatty acids (PUFAs), antioxidants, minerals, vitamins, and fibre (Bueno et al., 2018). The most recent revisions to Canada's Food Guide highlight the need to increase the percentage of protein in diets derived from plants, thus aligning with the global trend. Such a change in diet is especially important for Canada, the world's seventh-largest producer of soybeans, with an annual production of 6.5 million tonnes (Canada, 2022).

Shifting from culinary prominence to agricultural significance, soybeans are pivotal in bolstering sustainability. Their unique nitrogen-fixing ability, together with soil bacteria, reduces the need for nitrogen fertilisers, thus addressing a significant environmental concern about nitrogen fertilisers, one of many significant contributors to greenhouse gas emissions. Intensive breeding efforts to develop ever-earlier maturing soybean varieties have led to a remarkable extension of soybean cultivation in Canada. Despite these achievements, the soybean industry faces pressing challenges, in particular those due to increasing abiotic

stresses. The looming changes in climate for Canada's soybean-growing regions pose a substantial threat. Drought stress is a critical issue, impacting yields even in non-drought years. All of this emphasizes the need for innovative approaches and the urgency of research to enhance soybean resilience for food security and environmental sustainability (Brevedan & Egli, 2003; Morrison et al., 2006).

An avenue to address these challenges lies in developing soybean varieties with improved root systems. While roots are often considered the "hidden half" of the plant, their significance in nutrient and water acquisition cannot be understated (Atkinson et al., 2019). Root systems act as flexible and dynamic conduits, supplying nutrients and water to the plant and playing a pivotal role in crop adaptability to abiotic stressors such as drought and soil sub-optimal fertility. The ability of plants to mobilise nutrients in the soil through their root exudates is important. These exudates, which include organic compounds like sugars, amino acids, and organic acids, significantly influence soil pH and composition, thereby facilitating access to essential nutrients (Canarini et al., 2019; Lei et al., 2023).

As we investigate the complexity of soybean root systems, the specific focus on the Root System Architecture (RSA) becomes imperative. The search for soybean varieties with adaptable root systems that maximize crop growth and yield outputs, conserve resources, and withstand climatic change is intensifying (Hirai et al., 2004; Masclaux-Daubresse et al., 2014; Mochida & Shinozaki, 2010). The root systems of plants not only enable them to adapt to their surroundings and improve their uptake of nutrients and water (Alexandersson et al., 2014; Sriyudthsak et al., 2014), but they can also recognise and react to edaphic stressors, such as salinity, drought, and waterlogging, before other plant organs (Bylesjö et al., 2007; Casero et al., 1995; Furbank & Tester, 2011; Geigenberger et al., 2011; Lisec et al., 2006; Palmer et al., 2014; Tohge et al., 2014; Usadel et al., 2012; Yu et al., 2014). The impact of competition for resources, such as mobile and immobile nutrients and water, on the RSA through the form and

spatial organization of the plant root system has been well-documented. This impact is contingent upon the composition of the soil (Fitter, 1987; Lynch, 1995). Crop adaptations to drought, infertile soil, and other edaphic stressors depend heavily on modifications to the RSA encountered during the root system development (Casero et al., 1995). Thus, screening for and breeding crop cultivars with higher RSA that are more edaphic stress-tolerant and have superior nutrient and water uptake efficiency is crucial (Hodge et al., 2009; Waidmann et al., 2020).

The conventional approach to assessing RSA traits in plants grown in the field is known as "shovelomics." This method involves removing root systems from the soil and visually analysing them for characteristics that are relevant to the RSA (Trachsel et al., 2011). Non-destructive methods have been designed to overcome the drawbacks of this strategy, especially in controlled indoor environments. They may involve rhizoboxes or enclosures with removable or clear viewing windows (Atkinson et al., 2019). Soilless methods such as hydroponics (Ayalew et al., 2018; Hargreaves et al., 2009), aeroponics (Lakhiar et al., 2018; Osvald et al., 2001; Selvaraj et al., 2019), gel plates (Wojciechowski et al., 2009) and growth pouches (Adeleke et al., 2019; Adu et al., 2014; Hund et al., 2009) provide more contrast between the substrate and the roots. While these techniques allow direct imaging of the root system and the measurement of RSA traits in a given substrate, it must be noted that plants grown in an artificial substrate are likely to have different root systems than if they were grown in soil (Clark et al., 2013; Clark et al., 2011).

Most of these methods, however, produce two-dimensional (2D) data. When soil is utilised, the many aspects of the plant's RSA are not quantified and the three-dimensional (3D) structure, when the growth is happening in 3D space, fails to be captured (Topp et al., 2013).

To overcome this restriction, advanced imaging methods such as X-ray computed tomography (CT) scanning (Han et al., 2008, 2009; Mooney et al., 2012; Rogers et al., 2016; Subramanian et al., 2015), magnetic resonance imaging (Jahnke et al., 2009), and positron emission

tomography (Garbout et al., 2012) can be used to phenotype roots non-destructively in soil in 3D space. With the appropriate software for image processing and analysis, these cutting-edge technologies can offer a complete insight into the spatial organisation and structure of root systems within their native soil environments, enabling more precise and perceptive plant science studies by providing a thorough grasp of the RSA features.

Our innovative approach combines CT scanning technology and the estimation of fractal dimension (FD) in a spatial context, thus providing a nuanced understanding of soybean root branching patterns. Fractal geometry concepts have been applied to soybean leaf canopies to assess the complexity of branching patterns above ground (Foroutan-pour et al., 2001). As a complexity indicator, the FD is known to incorporate information from root length traits (Subramanian et al., 2015), adding to them information about the spatial distribution and roughness of roots; a root growing in a compact or dense soil tends to be less smooth or 'rough'. With the use of soil in pots to grow soybean plants in an open space near a greenhouse, our 3D phenotyping framework seeks to be closer to field conditions in terms of plant growth starting with seed planting. The soybean plants in the reported experiment were watered as needed, so no water stress was applied. This notwithstanding, the results can be used for comparisons with a former study with vermiculite in rhizoboxes and 137 soybean cultivars the thirty here and a field experiment (with versus without irrigation), which is part of the same team research project. Accordingly, this Master's thesis enhances plant phenotyping approaches, technologically and quantitatively, in the context of climate change.

Hypothesis

The overarching hypothesis guiding our thesis is: "Applying a protocol including a soil environment and a 3D phenotyping platform uncovers hidden aspects in the variation of the RSA among cultivars of the same crop."

Objectives

This hypothesis anchors three specific objectives:

- To develop an appropriate 3D phenotyping framework for accurately measuring and estimating RSA complexity in soybeans.
- To assess the genetic component of variation in RSA complexity among 30 soybean cultivars.
- To validate the use of FD, estimated from the reconstructed 3D image of a root system after CT scanning, for eventually applying it to identify climate-resilient soybean cultivars.

Chapter 2: Literature Review

2.1. Overview

As the demand for soybeans (*Glycine max*) rises because of their nutritional content and adaptability, improving crop resilience and production becomes even more important. The RSA affects a plant's capacity to absorb water and nutrients, adapt to environmental challenges, and contribute to agricultural productivity and efficiency eventually. Advancements in agricultural technology have brought about new ways to study plant RSAs, particularly through the use of 3D phenotyping techniques, and gain a better knowledge of the intricate structure and operation of root systems that 2D approaches may overlook.

Originally designed for medical diagnostics (Kalender, 2011), X-ray CT scanning technology has revolutionised how we can visualise and analyse the 3D structure of root systems in soils. This approach enables researchers to survey root growth and architecture graphically and quantitatively, offering key information for developing more resilient and productive crops. Furthermore, the application of mathematical models such as Fractal Geometry offers a unique way to describe the complexity of root systems. In particular, the FD aids in describing the complexities of root branching patterns and has the potential to help understand the plant's nutrient intake and stress response. The purpose of this literature review is to examine the current state of research on soybean RSA, with a specific focus on 3D phenotyping technologies and FD-based analysis. The review aims to explain how innovative phenotyping methodologies can contribute to the development of soybean cultivars with optimised root systems, ultimately improving crop performance and sustainability. The details of soybean RSA are first explored below.

2.2. Significance and Complexity of Soybean Root System Architecture

2.2.1. The soybean root system: An overview

Soybean (*Glycine max*) is a dicot plant having allorhizic roots (Fitter, 1987; Osmont et al., 2007). Allorhizic root systems are dominated by the main or primary root, from which lateral roots arise. Adventitious roots are rare in allorhizic systems, but occasionally emerge from the hypocotyl or stem in particular upon wounding. The main and lateral roots have an apex, which is their most active part and is essential for nutrient absorption. Usually, the roots are lined with root hairs, which have a lifespan of 1–2 weeks, in the mature area of the tip. After the root hairs die, new root hairs are generated in the elongation zone to supplement and change the position of roots in the soil to absorb nutrients (Piekarska-Stachowiak & Nakielski, 2013). Despite covering a very small portion (e.g., 3%) of the soil space, roots play a critical role in crop growth by actively seeking nutrients (Dayan et al., 2007; Kanase et al., 2019). The phenotypic categorisation of soybean varieties is primarily determined by their root morphology (Fried et al., 2019). The root morphology of soybean varieties exhibits, in fact, significant disparities that can be broadly categorised into three groups: (1) a well-developed primary root (taproot); (2) a non-prominent primary root; and (3) longer branched roots (Xiong et al., 2021). The root system structure of soybean seedlings mirrors the early bulging phase, with minor variations in the initial structure and the bulging stage's onset (Xiong et al., 2021). Gai et al. (2007) stress the importance of accurately and dynamically describing root morphology by considering the variability in elongation rates and root density.

2.2.2. Factors influencing the soybean root system architecture

Phenotypic plasticity and environmental adaptation:

Phenotypic plasticity, the ability of an organism to alter its phenotype in response to environmental changes (Bradshaw, 1965; Des Marais et al., 2013; Palmer et al., 2012; Sultan & Spencer, 2002; Via et al., 1995). In soybean, it is posited as a key adaptive mechanism,

enhancing environmental tolerance and enabling the plants to maintain productivity in increasingly variable climates. It follows that genotypically identical soybean plants can differ in RSA, depending on their macro- and microenvironments. This adaptive capacity can manifest through changes in root-to-shoot ratios in drought conditions, for example (Huang & Fry, 1998; Verslues et al., 2006), underscoring the dynamic interplay between plant genetics, root morphology, and environmental stressors.

Soil compaction and RSA modification:

Soil compaction is a prominent factor, significantly affecting the RSA (Correa et al., 2019). Compacted soil conditions lead to various effects, including reduced root length (Bingham et al., 2010; Grzesiak et al., 2002; Pfeifer et al., 2014), thicker root diameter (Eavis, 1972; Goss, 1977; Popova et al., 2016; Rich & Watt, 2013), less steep root angles (Colombi & Walter, 2015), and deflected growth (Chen et al., 2014). Such changes facilitate the plant's ability to navigate compacted soil layers, which is crucial for accessing deeper soil moisture. Plants already resistant to compaction have adaptations such as increased root diameter and higher tortuosity, which improve their exploration of the soil and adjustment to environmental stresses (Correa et al., 2019).

Internal and genetic factors:

Apart from environmental interferences, the RSA is influenced by internal factors, including hormonal balance (Fukaki & Tasaka, 2009), plant maturity (Aulakh et al., 2001), the gravitropic set-point angle (Malamy, 2005), and the plant's intrinsic responsiveness to these changes (Malamy, 2005). Crosstalk has been observed between the pathways of phosphorus-responsive gene transcription and phosphorus deficiency-induced root development (Sánchez-Calderón et al., 2006). These processes involve intricate signalling mechanisms of synthesis, transduction, and sensitivity of signals across numerous developmental genes (Giehl et al., 2014). Such internal factors introduce genetic variation that can mask the effects of individual

genes on specific RSA traits (Kuijken et al., 2015). The complexity in regulating root phenotypes is complicated by pleiotropy and genetic interactions such as crosstalk (mentioned above) and epistasis. For instance, the Root-ABA1 QTL (Quantitative Trait Loci), has been identified to contribute to root lodging resistance in tomato (Giuliani et al., 2005; Landi et al., 2007). Similarly, a genome-wide association study in rice (Kadam et al., 2017) led to the identification of a gene (SCARECROW/SHORTROOT) known to influence the RSA. Moreover, a study using soybean cultivars found that QTL regions accounting for 15% –25% of the phenotypic variation in RSA traits (essentially root length-related) contain two putative candidate genes (Seck et al., 2020). These genes have homology to genes previously identified as influencing RSA in other species. Furthermore, reports of interacting QTLs for root traits in rice, maize, and Arabidopsis highlighted the complexity of epistasis (Bouteillé et al., 2012; Zhang et al., 2001; Zhu et al., 2006). Ultimately, the intricate web of genetic interactions, combined with environmental influences, complicates the understanding and breeding for specific root traits due to the obscured effects of individual genes.

2.3. Current Methods and Challenges in Root System Architecture Analysis

There have been recent advancements in phenotyping methods for root traits, including 2D image analysis, cross-sectional anatomy, shovelomics, 3D photography, and tomography technologies, and these methods hold significant promise for breeding purposes (Kuijken et al., 2015). The complexity of root systems and their dynamic interaction with the environment have led to the adoption of advanced imaging technologies, such as X-ray CT scanning, magnetic resonance imaging, and ground penetrating radar, to study roots in laboratory and field conditions (Fan et al., 2022; Lafond et al., 2015; Morris et al., 2017; Rellán-Álvarez et al., 2015). These technologies already enabled the development of detailed 3D models for

quantifying RSA (Dunbabin & Postma, 2013), significantly advancing our understanding of root distribution and function under varying environmental conditions.

Focusing on the agronomic relevance of specific root traits, the soil is generally identified as the natural cultivation medium. Root systems developed hydroponically or in gellan gum exhibit significant differences compared with soil growth (Clark et al., 2011; Hargreaves et al., 2009; Wojciechowski et al., 2009), highlighting that artificial growth media do not reproduce field conditions. Therefore, the integration of soil environments in studies involving high-resolution imaging technologies is crucial for a realistic evaluation of root behaviour and the effective translation of laboratory findings to field applications, so that research remains relevant to actual agricultural practices.

Often, plants used for root phenotyping in soil are grown in soil-filled tubes or pots, flat cartridges, or regular soil environments under greenhouse conditions (Bucksch et al., 2014; Burton et al., 2012; Dresbøll et al., 2013; Nagel et al., 2009; Nagel et al., 2012; Ytting et al., 2014). One of the main challenges with these cultivation methods is soil heterogeneity, including composition and moisture, which can complicate the isolation of root systems from images considerably (Kuijken et al., 2015; Lontoc-Roy et al., 2006). Many researchers opt for artificial media used in indoor cultivation systems, which helps for higher throughput and more controlled conditions, thus reducing environmental noise. Common practices in these controlled environments include 2D rhizotron systems, such as growth pouches (Hund et al., 2009), between paper (Adu et al., 2014), rhizoboxes (Seck et al., 2020), or between fabric cloths in bins (Chen et al., 2011; Le Marié et al., 2014). These methods provide a more standardised micro-environment, which is crucial for accurate phenotyping and complements the detailed insights gained from advanced imaging techniques used in real soil conditions. However, these methods can force roots into an unnatural growth conformation and utilise media with chemical and physical properties that may not be representative of natural soil

conditions, presenting a notable limitation in their agronomical applicability. As a result, there are trade-offs in achieving high resolution, processing data efficiently, mimicking the real cultivation system, and measuring the desired root parameters comprehensively.

New high-throughput phenotyping platforms are designed to balance controlled environments with realistic root system modelling, and often utilise 2D imaging techniques with cameras (Clark et al., 2013; Le Marié et al., 2014; Nagel et al., 2009) or flatbed scanners (Adu et al., 2014; Chen et al., 2011; Hund et al., 2009; Slovak et al., 2014), to facilitate the observation and measurement of roots. These methods are user-friendly and allow for rapid data collection, but they do not adequately capture the intricate 3D structure of root systems and the process of untangling and flattening roots for 2D imaging can be both tedious and potentially harmful to the roots. Therefore, alternative approaches involve growing root systems in a 3D medium and using 2D optical cameras for imaging roots, with the images later reconstructed into 3D models to provide a more comprehensive view of the RSA (Douarre et al., 2016; Huang et al., 2023).

2.4. Computed Tomography Scanning in Plant Science

2.4.1. Overview

For root systems grown in soil, several 3D imaging techniques allow for the in-situ visualisation of roots without altering the bio- and physico-chemical properties, porosity, and mechanical resistance of the soil. The most notable among these methods is X-ray CT scanning, which provides detailed 3D and cross-sectional images of roots embedded in their soil environment, facilitating an accurate analysis of root structure and distribution without the disruptive process of extraction (Lafond et al., 2015; Mooney et al., 2012). Overall, these advancements in 3D imaging technologies provide valuable tools for overcoming the limitations of traditional 2D methods, enabling more precise and less invasive studies of root systems grown in soil environments mimicking the field reasonably well.

2.4.2. Basic Principles of X-ray CT Scanning

X-ray CT scanning is a non-destructive and non-invasive imaging technology that enables the visualisation of the internal structure of objects in 3D, and by cross-sectioning, in 2D. Its potential for use in the plant and soil sciences, including root visualisation, was explored in the 1980s-1990s (Aylmore, 1993; Crestana et al., 1986). In particular, the ability of X-ray CT scanning to detect both biotic and abiotic components effectively was demonstrated by (Tollner, 1991). Over the years, X-ray CT scanners have evolved significantly, improving functionality while maintaining the fundamental principles that define their operation. X-rays are generated in and emitted from a highly evacuated tube, usually called an "X-ray tube", containing two electrodes: a cathode and an anode, typically made of platinum or tungsten. Upon application of a high voltage (e.g., 60 kV and above for a macro-CT scanner), electrons accelerate from the cathode to the anode, emitting X-rays upon collision. As X-rays pass through the sample installed on the couch, they are partly absorbed or scattered by the material. This interaction is quantitatively described by the Beer-Lambert Law:

$$\boldsymbol{I = I_0\, exp(\mu\, Bd)} \qquad \textbf{\textit{Equation (1)}}$$

which relates the initial intensity (I_0) of the monochromatic radiation to the attenuated intensity (I) after passing through a sample with bulk density Bd; μ is the linear attenuation coefficient (Wildenschild et al., 2002). This law, through the derived CT numbers (see below), is fundamental in determining the density of the different parts of the sample based on the attenuation of the X-ray beam, providing detailed insight at a fine resolution into the internal structure of the sample without causing damage.

In medical (macro-) CT scanners, the X-ray tube and the detectors, on opposite sides of the gantry, encircle the patient (object), capturing multiple projections while the patient (object) comes in or out of the gantry depending on the exam plan, in a type of scan called "helical" since the early 2000s. Conversely, in non-medical (micro-) CT scanning applications, the

sample installed on a plate rotates between a stationary X-ray source and the detectors. From the raw projection images, 2D arrays (matrices) of "CT numbers" are computed with the appropriate algorithms provided by the CT scanner company. Typically, the 2D array size is 512 x 512 entries. Their packing without default, thanks to the helical scan, provides a 3D array, with a length (in entries) along the third axis equal to the physical length of the volume CT scanned, divided by the reconstruction interval length (usually in cm and a fraction of mm, respectively, for macro-CT scanners). The concept of pixel in 2D is thus extended to that of "voxel" in 3D; a voxel can be seen as a pixel with a certain depth equal to the reconstruction interval length.

As mentioned above, the reconstruction process from projection images to "CT images" (i.e., the 2D arrays) involves computing CT numbers (CTN), expressed in Hounsfield units (HU) (Kalender, 2011):

$$\boldsymbol{CTN(HU) = \frac{\mu\, voxel - \mu\, water}{\mu\, voxel - \mu\, air}\, times\, 1000} \qquad \textit{Equation (2)}$$

where μ *object* denotes the linear attenuation coefficient for the voxel; μ *water*, the linear attenuation coefficient of pure water; and μ *air*, the linear attenuation coefficient of a standardized air sample; μ *air* is expected to be 0.

One CTN is computed for each voxel, and its value is an indirect estimate of the material density of the corresponding part of the CT scanned volume. Traditionally, medical CT scanners are calibrated so that air CTN is equal to –1000 HU, water CTN to 0 HU, and bone CTN to +1000 HU. As a 512 x 512 grey-tone map of CTNs, a CT image has brighter and darker pixels, indicating higher X-ray attenuation (denser material) and lower X-ray attenuation (lighter material), respectively.

2.4.3. X-ray CT scanning for root growth visualisation in soil

X-ray CT scanning offers great potential for examining undisturbed RSA in the soil, and is less affected by soil paramagnetic elements than magnetic resonance imaging (Tollner et al., 1994). In the past two decades, X-ray CT scanning has been increasingly utilised in a wide range of studies, highlighting its versatility and effectiveness in capturing detailed internal structures non-invasively. The use of low-dose X-rays with medical CT scanners has been proven adequate for studying the development of plant structures, presenting a significant advantage over industrial CT scanners, which do not allow the same level of contrast and are lethal to plants due to much higher X-ray doses.

The effectiveness of the use of a macro-CT scanner with plants to study their structures, above ground (leaf canopies and branching patterns) and below ground (root systems) has been affirmed by the results of multiple studies, including (Dutilleul et al., 2008; Dutilleul et al., 2005; Han et al., 2008, 2009; Lontoc-Roy et al., 2005). Zappala et al. (2013), while analysing rice root traits and exploring the associated microbial communities, demonstrated that X-ray CT scanning did not significantly affect the biological attributes of their samples. Jenneson et al. (1999) initially documented the capacity of a micro-CT system to generate 3D time-lapse images of growing wheat seeds (*Triticum aestivum*) with a resolution of 100 μm. Gregory et al. (2003) repeated these micro-CT results for wheat, and obtained similar micro-CT results for rape (*Brassica napus*), both grown in a sandy loam. Lontoc-Roy et al. (2006) investigated the RSA of young maize seedlings grown in various soil conditions, using macro-CT. To identify the root material in the plant-soil CT scanning data, the authors applied an initial global CTN thresholding that was adjusted to the soil type and moisture content, underscoring the necessity of adaptive thresholding to achieve accurate image segmentation including root isolation.

Han et al. (2008) made a significant advancement in RSA analysis by successfully extracting the architecture of first-order potato (*Solanum tuberosum*) roots from CT data. Their

methodology employed an interactive system that allowed a human operator to manually track the root through a series of CT slices. This hands-on approach involved the operator marking the centre of the root region in each slice, which provided a direct and intuitive means of tracing the root's structure. This manual tracking method proved effective in identifying architectural variations in potato roots, especially those influenced by external biological factors. The study was able to discern differences in the root structures of plants that had been inoculated with a scab-inducing bacterium (*Streptomyces scabies* EF-35). These procedures integrate the precision of automated systems with the nuanced understanding of human operators, providing a more reliable and comprehensive analysis of root architecture.

CT scanning has revolutionised the visualisation and analysis of underground plant structures, but the inherent complexities of root architecture—such as overlapping roots, curves, and bends—often exceed the capabilities of conventional imaging techniques (Weihs et al., 2024). These complexities necessitate more sophisticated analytical approaches to understand root systems fully. Current techniques range from global or local thresholding to more advanced automated procedures that reduce operator bias, though these cannot entirely replace human judgment (Baveye et al., 2010). Technological advances, cost reductions in imaging and sensor platforms, and progress in AI subfields recently started to enhance plant breeding efforts by enabling faster, high-resolution sampling and analysis of root phenotypic data (Falk et al., 2020).

2.5. Fractal Dimension as Complexity Indicator in Root System Architecture Analysis

Fractal geometry, introduced by Mandelbrot (1982), describes irregular and complex structures that do not fit traditional Euclidean geometry and its integer dimensions (i.e., 1 for straight lines, 2 for planes, and for volumes). Fractals allow for non-integer dimensions, providing a more nuanced measurement of spatial complexity and space occupancy for patterns recurring

over multiple scales (Tatsumi et al., 1989; Walk et al., 2004; Wang et al., 2009). This property of self-similarity, where the form or pattern is consistent across scales, is particularly useful for studying natural structures, such as root systems (Dutilleul et al., 2008; Hauck et al., 2015).

The FD of structures meeting the fractal assumption can be estimated with a variety of methods, most notably the box-counting procedure for 2D images and the cube-counting procedure for 3D images. In the former, a grid of square boxes of decreasing sizes (starting with half the side of the smallest square containing the structure, divided by 2, 4, etc.) is superimposed onto the image and the number of boxes intersecting the structure of interest is counted for each size. Eventually, FD is estimated as the slope of the log-log plot of the number of intersecting boxes against the inverse of the box size (Foroutan-pour et al., 1999 b). Analogously, the cube-counting procedure is applied to 3D images, by using cubes instead of boxes to account for the volumetric intricacies of the structure (Dutilleul et al., 2015).

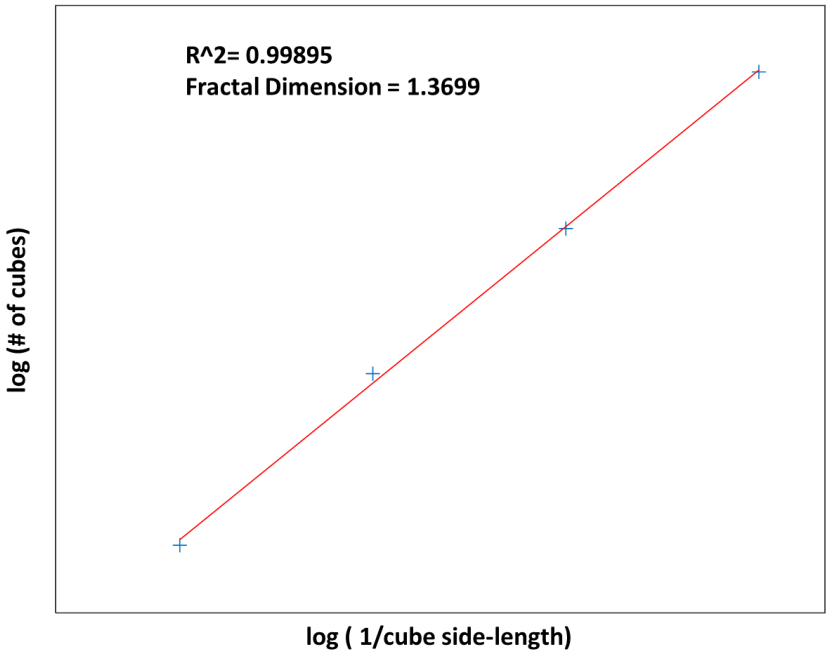

Figure 2.1: Example of log-log plot in the cube counting procedure for a soybean plant from the OAC-CHAMPION

Fractal analysis has been applied to assess the complexity of plant structures (branching patterns, root systems) in crop plants. For example, Foroutan-pour et al. (2001) explored the use of FD to quantify the complexity of soybean canopy architecture affected by population density and intercropping with corn. Estimated on soybean branching patterns from which leaves had been detached manually, Foroutan-pour et al. (2001) showed that FD correlated with changes in canopy architecture and increased over time as structural complexity was increasing during plant development. They also compared FD with traditional canopy growth metrics (e.g., leaf area), showing that FD provides new insights into the spatial distribution of leaves in the canopy for light interception and photosynthesis. The concept was similarly explored for root systems and confirmed by (Lontoc-Roy et al., 2006) and Subramanian et al. (2015), replacing leaf area above ground with root length underground and light interception with water and nutrient uptake. The root system FD in two rice cultivars was correlated with drought performance (Wang et al. (2009)), and observations of transgressive segregation in root system FD between maize recombinant populations suggest the presence of genetic variants in the parental inbreds that can either increase or decrease this characteristic (Grift et al., 2011).

Connecting Text

A preliminary study was imperative to enhance our understanding of the genetic determinants influencing RSA in soybean. For this purpose, we focused on evaluating phenotypic variation within a diverse germplasm pool consisting of 137 soybean lines (Seck et al., 2020). From this extensive dataset, a strategic subset of 30 cultivars was meticulously selected by multivariate statistical analysis, primarily cluster analysis. This method allowed the identification of representative soybean lines exhibiting distinct RSA traits, which will provide a basis for detailed 3D phenotyping. In Chapter 3 and the derived publication (Sanghera et al., 2023), a robust framework is developed by applying cluster analysis with various criteria, to determine representative lines that can be used in the experimental work presented in Chapter 4.

Chapter 3: Cluster Analysis of 137 Soybean Lines Based on Root System Architecture Traits Measured in Rhizoboxes

Prabhjot Sanghera[1], François Belzile[2], Waldiodio Seck[2,] , and Pierre Dutilleul[1]*

[1]Department of Plant Science, McGill University, Macdonald Campus, Sainte-Anne-de-Bellevue, QC, Canada

[2]Département de phytologie et Institut de biologie intégrative et des systèmes, Université Laval, Québec, QC, Canada

Research Paper was derived from this chapter in the following publication

Sanghera, Prabhjot, François Belzile, Waldiodio Seck and Pierre Dutilleul. "Cluster Analysis of 137 Soybean Lines Based on Root System Architecture Traits Measured in Rhizoboxes." J Biom Biosta 14 (2023): 179.

DOI: 10.37421/2155-6180.2023.14.179

3.1. Abstract

The reported study was motivated by the necessity to select 30 soybean lines from a total of 137 for a sophisticated 3-D phenotyping analysis of the Root System Architecture (RSA), which would not allow that all the lines be included and replicated. A representative subset of size 30 was found after performing four cluster analyses and comparing the results of two more particularly. These two cluster analyses are based on the data for 12 RSA-related traits previously collected in 2D on three replicates of the 137 soybean lines and the first six principal components representing 95% of the total dispersion after data standardization in a preliminary Principal Component Analysis (PCA). The two cluster analysis procedures provided 16 soybean lines that were the closest to the centroid of their respective cluster in both cases. Fourteen more were found to be common and at a distance from the centroid below a pre-set threshold value without being the closest. The final selection of 30 excludes two soybean lines that were the second member selected from their cluster, and includes instead two soybean lines that are the closest and second closest to their respective centroid in the cluster analysis after PCA on standardized data, but are not well represented in the other cluster analysis. In conclusion, the 93.3% overlap between the two sets of results shows a robust clustering structure in RSA 2-D phenotyping in soybean. Our statistical approaches and procedures can be followed and applied in other biological frameworks than plant phenotyping.

Keywords: Cluster analysis • Data standardization • Distance to the centroid • Plant phenotyping • Principal component analysis • Root system architecture

3.2. Introduction

One of the main difficulties in experimental research of biological systems is the bidirectional relationship between genotype and phenotype [1-7]. Researchers in the omics sciences, including phenomics [8], are continuously developing new technologies that produce enormous amounts of data, which help improve our understanding of the complexity of living organisms provided they are analysed appropriately. To enable drawing biologically relevant conclusions, statistical methods, among others [9-12] must be optimized in parallel. To share raw data from omics experiments, they are presented in figures and visualized with meaningful representations. The primary goal of agricultural phenomics, or field omics [13], is to measure and compare phenotypes of crop plants. With the interpretation of dendrograms and proximity to centroids, cluster analysis represents a potential, very effective means to meet that objective. Different clustering algorithms exist that can, for given criteria, group individuals and identify them as cluster members [14].

Phenotypic variation in a germplasm pool is necessary for plant breeders to progress through selection. In this study, we have analysed phenotypic data for the Root System Architecture (RSA) of 137 soybean lines; source of data:[15]. The primary or tap root is the first organ formed by hypophysis in germinating seeds [16]. The thick soybean primary root produces primordia from the pericyclic cells, which grow into lateral roots [17]. Numerical variables, such as the quantity of secondary lateral roots, average root diameter, and root length, typically describe the size and abundance of the root system components. In other measured variables, the focus is on the topology or structure of the root system, like the type and angle of root connections [18]. Here, 12 RSA-related traits had previously been measured from 2-D images of the content of rhizoboxes in which soybean seedlings were grown: Total Length of Roots (TLR), Length of Primary Root (LPR), Length of Secondary Roots (LSR), Distribution of Total Root Length (DTLR), Total Number of Roots (TNR), Median number of roots (Med),

Maximum Number of Roots (Max), Depth of Root System (DRS), Width of Root System (WRS), Surface of Root System (SRS), Diameter of Primary Roots (DR), and Surface Area of primary Root (SAR) [15]. We first performed cluster analysis on the dataset introduced above in four ways: without vs. with data standardization, combined or not with the application of a Principal Component Analysis (PCA) to reduce data dimensionality, and then focused on two ways called "Approach 1" and "Approach 2". In doing so, our motivation was to answer best the questions: How to analyse RSA multivariate data to objectively define a given number (e.g., 30) of clusters? How can a relevant member (i.e., a soybean line) be identified for each of the 30 clusters? These questions are addressed while keeping in mind that the resulting 30 soybean lines would later be used for a sophisticated, time-consuming RSA phenotyping in 3D. We used the SAS software, Version 9.4 for Windows (SAS Institute Inc.,Cary, NC, USA), to design and perform our cluster analyses.

3.3. Materials and Methods

Source of experimental data

The dataset used in the multivariate analyses described below consists of the mean values of phenotypic data collected for three seedlings per line (N=3) from 137 lines of soybean grown in Canada. The seeds were first germinated in Petri dishes filled with fine vermiculite and then transplanted into custom-designed rhizoboxes filled with vermiculite. After 10 days of growth, images of the roots were taken using a camera. The Automatic Root Image Analysis (ARIA) software was used to extract the RSA-related traits from each 2-D image: TLR, LPR, LSR, DTLR, TNR, Med, Max, DRS, WRS, SRS, DR, and SAR [15].

Cluster analysis

This multivariate statistical method is aimed at identifying “clusters”, or groups of individuals, and their “members” for given criteria of proximity in the multidimensional space of a quantitative dataset. In the plethora of existing cluster analysis procedures, clustering depends on the definition of proximity and the type of distance or similarity involved; see, e.g.,[14]. In all cases, the basic principles of the method are the same: grouping individuals that are more similar in the same cluster around a “centroid”, in a way that maximizes the separation among clusters while minimizing the distances between members within clusters.We applied cluster analysis to obtain 30 clusters from 137 soybean lines (1 individual=1 soybean line). As a starting point in a given approach, we identified the soybean lines with greatest proximity to the centroid as representatives of the clusters. Our motivation is to select objectively 30 soybean lines for future research work that is practically impossible to undertake with all the 137 soybean lines (i.e., RSA phenotyping based on computed tomography scanning). In this study, we performed disjoint cluster analyses with the SAS procedure FASTCLUS, in which a nearest centroid sorting algorithm is implemented. We used it without the option of cluster seeds as first guess for centroids, so that the algorithm initially considered each individual as a separate cluster. Distances between two individuals, between one individual and the centroid of one cluster with more than one member, and between two centroids of clusters with several members were computed based on the values of the input variables (using means when centroids of non-singleton clusters are involved); see the VAR statement in SAS scripts A1 and A3 in the appendix. By default, the Euclidean distance is used to assess the proximity among individuals and clusters. The algorithm merges the two closest clusters at each step until the desired number of clusters (MAXC) is reached. Unlike the SAS procedure CLUSTER, PROC FASTCLUS assigns each individual to a single cluster without organization in a hierarchical tree structure. We developed and followed two approaches for clustering.

Approach 1: Cluster analysis with the 12 RSA-related traits. In SAS script A1, "MAXC=30" specifies the requested number of clusters, and the final cluster assignments are saved as output in "work.fastclus_scores".

Approach 2: Cluster analysis with 6 principal components (Prin1-Prin6). In this approach, results of a preliminary PCA are used; see the text below and SAS scripts A2 and A3. The input variables VAR in A3 are "Prin1-Prin6". These were chosen for cluster analysis after PCA (see below) showed that they accounted for 95% of the variability in the data table after column standardization. Prior to standardization, the data table (with 137 rows and 12 columns) contained the mean values (N=3) per soybean line for each of the 12 RSA-related traits. The other options in A3 (i.e., MAXC, OUT) are the same as in A1.

Principal component analysis

That multivariate statistical method can be performed on the same dataset as cluster analysis, but has a different aim than cluster analysis. PCA is used to examine the relationships among quantitative variables observed on a number of individuals in order to reduce dimensionality of the data space [14]. Matrix algebra tools applied to the sample correlation matrix (with ones as diagonal entries and standardized covariances off the diagonal) provides “principal components” based on eigenvalues and associated orthogonal eigenvectors. By performing PCA, we aimed to identify structural patterns in association of the 12 RSA-related traits over the 137 soybean lines and assess differences in cluster analysis results obtained with well-defined principal components (Approach 2) vs. with no data standardization and no dimensionality reduction (Approach 1). In SAS script A2 in the appendix, the procedure PRINCOMP is called with "DATA=PCA_Seck_et_al_2020" to specify the input dataset and the option STANDARD to perform PCA on the 12 × 12 sample correlation matrix (i.e., after transforming the data for each variable to a sample variance of 1.0). The latter option facilitates the interpretation of results by focusing on associations among variables via correlations, while

avoiding scale effects related to data dispersion and measurement units if the 12 × 12 sample variance-covariance matrix was used.

3.4. Results and Discussion

The first 6 principal components (out of a maximum of 12; there are 12 variables provided by the 12 soybean root traits) explain about 95% of the variability in the data table (Figure 3.1, top left panel). Several of the RSA-related traits are redundant; see SAR, DRS, DTLR, LSR, TLR and WRS, RS in the PCA biplots (Figure 3.1, other panels). The latter result confirms the correlation analysis results reported in (Seck et al., 2020).

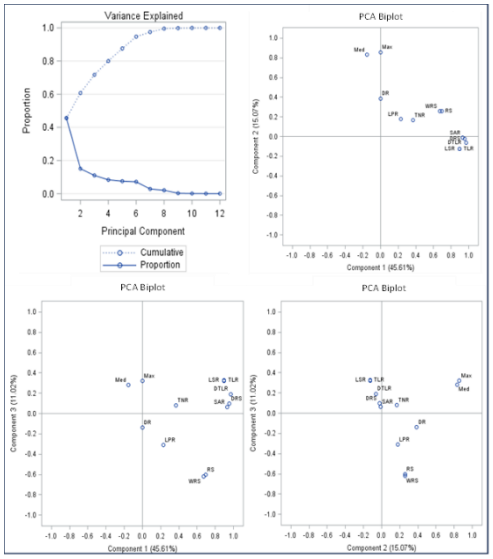

Figure 3.1: Principal component analysis (PCA) results.

Top left panel: Percentage of the variability in the data table explained by the 12 principal components, cumulatively and non-cumulatively. Other panels: Biplots of Prin2 against Prin1, Prin3 against Prin1, and Prin3

against Prin2; Prin1, Prin2, Prin3 denote the first three principal components in descending order of the associated eigenvalues.

In a PCA with standardization of the data table, which is equivalent to performing the PCA on the sample correlation matrix [14], "variance", "dispersion", "variation", and "variability" tend to mean the same thing. Using the criterion of greatest proximity or smallest distance to the centroid, 16 soybean lines are found to be common to the lists of 30 names obtained in the cluster analyses along Approach 1 and Approach 2; see the yellow highlights in Table 3.1.

Table 3.1: A summary of the initial cluster analysis results obtained in Approach 1 and Approach 2

Analysis with the 12 RSA-related traits			Analysis with Prin1-Prin6		
Cluster	Soybean line	Distance to the centroid	Cluster	Soybean line	Distance to the centroid
1	4004P4J	1.232596	1	4004P4J	1.330548
2	4005_24j	0.000000	2	4005_24j	0.000000
3	PS44	0.969116	3	PS44	0.903904
4	Jari	1.385713	4	OAC 7-26C	1.124655
5	Tundra	0.000000	5	Gretna	1.020093
6	Delta	0.000000	6	Madoc	0.844417
7	OAC 7-26C	1.222566	7	OAC Prudence	1.121011
8	Casino	1.379225	8	OAC Wallace	0.944889
9	5055_43G	0.000000	9	5055_43G	1.239143
10	Costaud	1.251672	10	Costaud	1.105240
11	Madoc	1.357312	11	Mandarin	0.929683
12	Maple Ambr	1.103940	12	Venus	0.000000

13	OAC 8-21C	0.898254	13	OAC 7-6C	0.000000
14	Woodstock	0.000000	14	Maple Glen	1.025438
15	S05-T6	1.191081	15	Bravor	1.111696
16	Albinos	1.447583	16	Tundra	0.000000
17	OAC 9-35C	1.088592	17	SECAN8-1	1.026367
18	Clinton	1.169068	18	Woodstock	0.000000
19	Maple Isle	1.057824	19	Jutra	0.775305
20	OAC Oxford	1.118181	20	OT94-47	0.728379
21	S14-P6	1.081495	21	Alta	0.651441
22	McCall	1.275310	22	McCall	1.090354
23	Gentleman	1.505267	23	4067P17j	1.107881
24	Flambeau	1.091571	24	S03-W4	0.000000
25	OAC 7-6C	0.000000	25	Roland	0.975369
26	OAC Wallace	0.954529	26	Maple Belle	1.015101
27	S03-W4	0.000000	27	OAC 7-4C	0.812049
28	Venus	0.000000	28	S14-P6	1.002491
29	Gaillard	0.844357	29	Mario	0.924578
30	OAC 7-4C	0.998249	30	OT05-20	1.209572

Approach 1 (Analysis with the 12 RSA-related traits) and Approach 2 (Analysis with Prin1-Prin6). Only the soybean lines that are the closest to the centroid of the cluster that they are a member of are listed. Those that are highlighted in yellow appear in both lists. Complete results are archived in Appendix Tables B1 and B2.

Loosening the required proximity to a maximum difference of 0.15 with the smallest distance to the centroid on both sides, 14 more lines were found to be common and at a distance from the centroid below 0.15 without being the closest. The final selection of 30 (Table 3.2) excludes two soybean lines (Madoc, McCall) that were the second member selected from their cluster, and includes instead two soybean lines (Mandarin, Maple Arrow) that are the closest and second closest to their respective centroid in Approach 2, but are not well represented in Approach 1.

Table 3.2: Final selection of 30 soybean lines

Sno	Genotype
1	4004P4J
2	4005_24J
3	5055_43G
4	AC2001
5	Albinos
6	Casino
7	Clinton
8	Costaud
9	Delta
10	Elora
11	Gaillard
12	Gentleman
13	Mandarin
14	Maple arrow
15	OAC 7-26C

16	**OAC 7-4C**
17	**OAC7-6C**
18	**OAC 8-21C**
19	**OAC 9-22C**
20	**OAC 9-35C**
21	**OAC Oxford**
22	**OAC Wallace**
23	**PS44**
24	**Proteus**
25	**S03-W4**
26	**S14-P6**
27	**SECAN7-27**
28	**Tundra**
29	**Venus**
30	**Woodstock**

Based on their membership of one of the 30 clusters identified in Approach 1 (Analysis with 12 root traits) and Approach 2 (Analysis with Prin1-Prin6) and their distance from the centroid. The 14 soybean lines highlighted in yellow here were also highlighted in yellow in Table 3.1; see text and Appendix Tables B1 and B2 for the selection of the other 16 soybean lines. In particular, Madoc and McCall, which are highlighted in yellow in Table 3.1, were eventually discarded to keep not more than one member per cluster after merging the two sets of cluster analysis results.

The reported overlap of 93.3% [i.e., (16+14–2)/30=0.933] shows a robust clustering structure in RSA 2-D phenotyping in soybean. Thus, we compiled, in a rational way, a list of 30 representative soybean lines with distinct RSA patterns that provide a good basis for 3-D investigation. Of course, germination tests with available seed banks as well as preliminary tests with growing media other than vermiculite justify adjustments to that list later. It is worth mentioning that OAC Bayfield readily provides a substitute to OAC 7-26C if required, as these soybean lines belong to the same cluster with two members in both approaches (Appendix Tables B1 and Table B2); they are therefore at equal distance from the centroid and either can be randomly picked. A comparison with genomic clustering results falls beyond the scope of a Brief Report, but could be the topic of another, broader study.

3.5. Conclusion

The selected 30 soybean lines will be used in RSA phenotyping with state-of-the-art equipment, followed by sophisticated 3-D data and image analyses. Selecting representative lines that showcase the diversity in root system architecture and possess biological relevance is crucial. The soybean lines in Table 3.2 are objective starting points for further investigation into the functionality of specific RSA-related traits on plant performance and adaptation. Our cluster analysis results provide insight into phenotypic variation within the germplasm pool. Understanding root system diversity is crucial for breeders aiming to progress through selection. Advanced 3-D phenotypic analyses, e.g., based on computed tomography scanning, is expected to deepen our understanding of the RSA and its impact on plant productivity and stress tolerance.

3.6. References

1. Mochida, Keiichi and Kazuo Shinozaki. "Genomics and bioinformatics resources for crop improvement." Plant Cell Physiol 51 (2010): 497-523.
2. Masclaux-Daubresse, Céline, Gilles Clément, Pauline Anne and Jean-Marc Routaboul, et al. "Stitching together the multiple dimensions of autophagy using metabolomics and transcriptomics reveals impacts on metabolism, development,and plant responses to the environment in Arabidopsis." Plant Cell 26 (2014): 1857-1877.
3. Hirai, Masami Yokota, Mitsuru Yano, Dayan B. Goodenowe and Shigehiko Kanaya, et al. "Integration of transcriptomics and metabolomics for understanding of global responses to nutritional stresses in Arabidopsis thaliana." Proc Natl Acad Sci 101 (2004): 10205-10210.
4. Usadel, Björn, Rainer Schwacke, Axel Nagel and Birgit Kersten. "GabiPD– the GABI primary database integrates plant proteomic data with gene-centric information." Front Plant Sci 3 (2012): 154.
5. Tohge, Takayuki, Leonardo Perez de Souza and Alisdair R. Fernie. "Genomeenabled plant metabolomics." J Chromatogr B 966 (2014): 7-20. 6. Palmer, Lachlan James, Daniel Anthony Dias, Berin Boughton and Ute Roessner,et al. "Metabolite profiling of wheat (T. aestivum L.) phloem exudate." Plant Methods 10 (2014): 1-9.
7. Lisec, Jan, Nicolas Schauer, Joachim Kopka and Lothar Willmitzer, et al. "Gas chromatography mass spectrometry–based metabolite profiling in plants." Nat Protoc 1 (2006): 387-396.
8. Furbank, Robert T. and Mark Tester. "Phenomics-technologies to relieve the phenotyping bottleneck." Trends Plant Sc 16 (2011): 635-644.

9. Sriyudthsak, Kansuporn, Michio Iwata, Masami Yokota Hirai and Fumihide Shiraishi. "PENDISC: A simple method for constructing a mathematical model from time-series data of metabolite concentrations." Bull Math Biol 76 (2014): 1333- 1351.

10. Bylesjö, Max, Daniel Eriksson, Miyako Kusano and Thomas Moritz, et al. "Data integration in plant biology: The O2PLS method for combined modeling of transcript and metabolite data." Plant J 52 (2007): 1181-1191.

11. Yu, Yong-Jie, Qiao-Ling Xia, Sheng Wang and Bing Wang, et al. "Chemometric strategy for automatic chromatographic peak detection and background drift correction in chromatographic data." J Chromatogr A 1359 (2014): 262-270.

12. Geigenberger, Peter, Axel Tiessen and Jörg Meurer. "Use of non-aqueous fractionation and metabolomics to study chloroplast function in Arabidopsis." Chloroplast Research in Arabidopsis: Methods and Protocols, Volume II (2011): 135-160.

13. Alexandersson, Erik, Dan Jacobson, Melané A. Vivier and Wolfram Weckwerth, et al. "Field-omics-understanding large-scale molecular data from field crops." Front Plant Sci 5 (2014): 286.

14. Morrison, D. F. "Matrix algebra." Multivariate statistical methods, 3rd edition.McGraw-Hill, New York, vii (1990): 36-78.

15. Seck, Waldiodio, Davoud Torkamaneh and François Belzile. "Comprehensive genome-wide association analysis reveals the genetic basis of root system architecture in soybean." Front Plant Sci 11 (2020): 590740.

16. De Smet, Ive, Steffen Lau, Ulrike Mayer and Gerd Jürgens. "Embryogenesis-the humble beginnings of plant life." Plant J 61 (2010): 959-970.

17. Lucas, Mikaël, Kim Kenobi, Daniel Von Wangenheim and Ute Voβ, et al. "Lateral root morphogenesis is dependent on the mechanical properties of the overlaying tissues." Proc Natl Acad Sci 110 (2013): 5229-5234.

18. Hodge, Angela, Graziella Berta, Claude Doussan and Francisco Merchan, et al. "Plant root growth, architecture and function." (2009): 153-187.

Connecting text

After establishing the basis in Chapter 3 for selecting 30 diverse and representative soybean lines from 2D work with plants grown in vermiculite, the transition to a detailed exploration of these 30 lines (with a few substitutions) is performed in Chapter 4, using advanced 3D phenotyping techniques (CT scanning) and plants grown in sand. This phase of our research leverages (i) X-ray CT scanning technology to visualise the structural complexity of the soybean root systems in 3D and (ii) CT scanning data and reconstructed 3D images to quantify this complexity by an appropriate fractal analysis. In this framework, the estimation of FD for individual plants across the selected soybean lines is susceptible of highlighting phenotypic variation in RSA among and within lines, more than in previous 2D work. With FD as a metric incorporating several other root measurements (lengths, angles), we aim to advance our understanding of the RSA and its importance for developing climate-resilient soybeans.

Chapter 4: Developing an Appropriate 3D Phenotyping Framework and Establishing Fractal Dimension as Complexity Indicator for Soybean Root System Architecture

Prabhjot Sanghera[1], Liwen Han[1], Donald L. Smith[1], François Belzile[2], and Pierre Dutilleul[1]

[1] Department of Plant Science, McGill University, Macdonald Campus, Sainte-Anne-de-Bellevue, QC, Canada

[2] Département de phytologie et Institut de biologie intégrative et des systèmes, Université Laval, Québec, QC, Canada

A manuscript will be derived from this chapter and submitted for publication as an Original Research article in a peer-reviewed journal.

4.1. Abstract

Understanding differences in root system architecture (RSA) is crucial for improving the resource-use efficiency of crops and developing climate-resilient cultivars. When underground, which is generally the case in nature, roots are challenging to observe and characterise. Here, we assessed the potential of the fractal dimension (FD) as an indicator of structural complexity in the root systems of 30 soybean cultivars grown in pots filled with sand for ~3 weeks. We used computed tomography (CT) scanning technology for non-invasive observation. After processing CT images and constructing 3D images of the isolated root systems for 110 plants, FD was estimated with the cube-counting procedure for each root system individually. The one-way analysis of variance performed on the FD estimates revealed a statistically significant ($P = 0.0192$) variation among the 30 soybean cultivars, as well as an important portion (60.3%) of the total variation related to individual plant effects within cultivars. Pairwise comparisons of FD mean values between cultivars and visual graphical inspection completed the interpretation of the observed phenotypic diversity in the RSA of soybean. The 3D results obtained here are compared with the 2D results obtained in a former study, and similarities and dissimilarities are discussed. In conclusion, advancements from 2D to 3D RSA phenotyping are underscored and FD is validated as an integrative indicator of root system complexity, of which the estimation requires less computing time than the measurement of root lengths and angles of multiple types. Accordingly, the inclusion of FD can be recommended in analyses with genetic data to develop climate-resilient soybean cultivars, thus promoting agricultural sustainability.

Keywords: root system architecture, soybean, phenotypic variation, 3D phenotyping, complexity, fractal dimension, stress resilience

4.2. Introduction

Soybean (*Glycine max*), alias “golden bean”, has proved to be a prominent source of protein both for humans and animals, and is widely recognised for its substantial contributions to bioenergy (Islam et al., 2019; Singh et al., 2018). Originally from Asia, soybeans are now cultivated globally, valued for their high protein and oil contents surpassing wheat, rice, and maize, and pivotal in bolstering sustainability thanks to their unique nitrogen-fixing ability, which reduces the need for nitrogen fertilisation (Brevedan & Egli, 2003; Morrison et al., 2006). They are emerging as protagonists in an unfolding narrative of global changes, resilience, and innovation. The soybean industry faces challenges, particularly abiotic stresses exacerbated by climate change (e.g., more frequent and longer droughts), which critically impact yields (Brevedan & Egli, 2003; Morrison et al., 2006). This situation underscores the urgency of research aimed at enhancing soybean resilience for food security and environmental sustainability.

One promising avenue is the development of soybean varieties with improved root systems, as roots, often called the "hidden half" of a plant, play a crucial role in nutrient and water acquisition, thereby significantly influencing crop's ability to sustain abiotic stressors (Atkinson et al., 2019). Root systems are adaptable and dynamic, and can substantially enhance a crop's ability to withstand abiotic stressors such as drought and poor soil fertility. Therefore, focusing on the root system architecture (RSA) in research and understanding its genetic determinants is imperative. The conventional approach to assess RSA traits in plants grown in the field is known as “shovelomics”. This method involves removing root systems from the soil and visually analysing them for characteristics that are relevant to the RSA (Trachsel et al., 2011). Non-destructive methods have been designed to overcome the drawbacks of this strategy, including soilless methods such as hydroponics (Ayalew et al., 2018; Hargreaves et al., 2009), aeroponics (Lakhiar et al., 2018; Osvald et al., 2001; Selvaraj et al., 2019), gel plates

(Wojciechowski et al., 2009), and growth pouches (Adeleke et al., 2019; Adu et al., 2014; Hund et al., 2009), or they involve rhizoboxes (Seck et al., 2020) or enclosures with removable or clear viewing windows (Atkinson et al., 2019).

The approaches above, however important, fall short of quantifying the RSA complexity in 3D. To overcome this limitation, we proceeded in two steps. First, we used the advanced imaging technology of computed tomography (CT) scanning (Han et al., 2008, 2009; Mooney et al., 2012; Rogers et al., 2016; Subramanian et al., 2015), and then, from the CT images duly processed, we performed a fractal analysis that provided one fractal dimension (FD) per root system. Our research work targeted the RSA phenotypic variation in the diverse germplasm pool of 137 soybean lines presented by (Seck et al., 2020). On this extensive 2D dataset, we performed cluster analysis to select a strategic subset of 30 soybean cultivars identified as distinct and representative of the whole set (Sanghera et al., 2023). In summary, our innovative approach combines CT scanning technology and the estimation of fractal dimension (FD) in a 3D spatial context, thus providing a realistic and detailed understanding of soybean root branching patterns. With the use of soil in pots to grow soybean plants in an open space near a greenhouse, our 3D phenotyping framework seeks to be closer to field conditions in terms of plant growth, starting with sowing. Accordingly, an enhanced plant phenotyping approach is presented hereafter, technologically, and quantitatively.

4.3. Materials and Methods

4.3.1. Growing Plants

Choice of Growing Medium:

Artificial materials may distort root growth into unnatural shapes and their chemical and physical characteristics do not mirror those of natural soil, thus limiting their practical agricultural use. Alternatively, the use of soil as a growing medium generally presents

heterogeneity, including composition and moisture, which can complicate the isolation of root systems from CT images (Kuijken et al., 2015; Lontoc-Roy et al., 2006). Therefore, we chose sieved homogeneous sand for growing our plants because of two advantages: it more closely approximates natural soil conditions, though it is not entirely similar, and it enhances the contrast between the roots and the surrounding medium in CT images, thereby reducing the difficulty in root isolation.

Sowing:

The seeds of the 30 experimental soybean cultivars (Table 4.1) and more were sourced in the laboratory of Prof. François Belzile at Université Laval. The final selection of 30 cultivars was based on the results of germination tests, depending on the success rate of germination in a sand medium. So doing, the cultivars second closest to the centroid in Sanghera et al. (2023) were accepted as replacements for those showing shy germination; for example, cultivar Elora in Cluster 30 was replaced by Drayton, to ensure germination as uniform as possible and a sufficient sample size.

The seeds were directly sown in sand-filled 15 cm diameter pots, 8 replicates per cultivar to begin with. Watering schedules were adjusted to lower the moisture content in the sand medium for CT scanning. This procedure enhances the contrast between the roots and the sand in the CT images, thereby improving their quality and optimising their analysis (Subramanian et al., 2015). The four potted plants with the most vigorous apparent growth above ground, for a given cultivar, were singled out and brought by van to the Macdonald Campus of McGill University (Sainte-Anne-de-Bellevue, QC, Canada).

Table 4.1: The final list of 30 soybean cultivars retained for experimentation, following germination tests

Cluster	Genotype
1	4004P4J
2	4005_24J
3	PS44
4	OAC 7-26C
5	AC2001
6	Casino
7	Saska
8	OAC Wallace
9	505543G
10	Costaud
11	MapleDonovan
12	Venus
13	OAC 7-6C
14	OAC Champion
15	OAC 9-22C
16	Tundra
17	OAC 1-26C
18	Woodstock
19	Dundas
20	OAC 8-21C
21	ACGlengary

22	McCall
23	Gentleman
24	S03-W4
25	OAC Oxford
26	OAC Kent
27	OAC 7-4C
28	Walton
29	Gaillard
30	Drayton

4.3.2. CT Scanning, Data Collection and Image Processing, Fractal Analysis

CT Scanning:

The plants were CT scanned at the Macdonald Campus of McGill University (Sainte-Anne-de-Bellevue, QC, Canada) in the CT Scanning Laboratory for agricultural and environmental research, using a Canon Aquilion Prime SP CT scanner (Canon Medical Systems Corporation, Otawara, Tochigi, Japan). For the reported study, all the seedlings were CT scanned on September 27, 2023, that is, almost three weeks after the seeds had been planted in the pots. The four pots per soybean cultivar were CT scanned together, in stand-up position, aligned in a row on the couch. The Helical Scan mode was used with an image reconstruction interval length of 0.5 mm along the Z-axis. The X-ray source settings were: voltage, 120 kV, and current, 100 mA. The field of view SS (24 cm in diameter) was used, with a zoom factor of 1.74, which provided a 0.27-mm resolution in the X-Y plane. About 300 cross-sectional CT images were reconstructed per potted plant.

Data Collection and Image Processing:

The pack of ~300 CT images for one soybean plant was analysed using customised functions written in MATLAB R2022b (The MathWorks Inc., Natick, MA, USA). Voxels (3D extension of pixels), likely containing root, were isolated on the basis of their CT number (CTN; in Hounsfield units, HU), an indirect measure of material density. No definite range of CTN values corresponds to roots, even for plants of a given species in a specific growing medium. Therefore, histograms of CTNs for the content (sand, roots) of CT scanned pots were built and inspected, looking for an appropriate interval of CTNs for roots on the left of the dominant peak for sand (Han et al., 2008, 2009) It thus appeared that appropriate intervals of CTNs for roots varied from [–600, 600] to [–350, 600]. Thereafter, the 3D array of CTNs was binarised: 1 = the voxel has a CTN in the interval and 0 = it does not, and the MATLAB function *volume list* was used to select the connected voxels considered to be parts of a root. Starting with the largest set of connected root voxels (likely the main part of the tap root, and parts of a few finer roots), 3D layers were added by decreasing the lower bound of the interval of root CTNs by multiples of 25 HU until no more root voxel could be attached. This procedure ensured that all the voxels considered to be part of the root system were connected horizontally, vertically, and diagonally. The final 3D image with the tap root and finer (generally lateral) roots was retained for further processing.

The final 3D image of each isolated root system was skeletonised by reducing each root (tap or finer) in the image to a thickness of one voxel. Foroutan-pour et al. (1999 a) highlighted the importance of skeletonisation as an essential step in many image-processing tasks, including the quantification of pertinent information contained in the image. Skeletal images capture all the structural parameters that affect FD and therefore provide support for FD estimation with a box-counting procedure in 2D (Foroutan-pour et al., 1999 b). The skeletonisation in 3D was performed with the image analysis toolset ImageJ (National Institutes of Health, Bethesda, MD,

USA). Eventually, any noise or unwanted structure left or introduced by the ImageJ skeletonisation procedure was eliminated by a final cleaning in MATLAB (Figure C1).

Fractal Analysis:

The skeletal 3D images of root systems of CT scanned soybean plants were subjected to FD estimation when the quantity of roots justified a fractal analysis. A customised programme written in MATLAB ((Han et al., 2008); Subramanian et al. (2015) was used for FD estimation. In this MATLAB programme, a binary array representing the 3D skeletal image of a root system is read as input. The cube counting procedure for FD estimation (Mandelbrot, 1982) is based on the counting of the cubes intersecting the skeletal image for cubes with a side length decreasing from half of the side length of the smallest cube containing the whole skeletal root system, divided by 2, 4, …, down to 2 voxels. Then, the natural logarithm of the number of intersecting cubes counted for side length s, log[N(s)], is plotted against log(1/s), and a straight line with slope D and an intercept is fitted by ordinary least squares:

$$\boldsymbol{log}\,[\boldsymbol{N(s)}] = \boldsymbol{log}\,\boldsymbol{K} + \boldsymbol{D}\,\boldsymbol{log}\,[\tfrac{\boldsymbol{1}}{\boldsymbol{s}}] \qquad \textit{Equation (3)}$$

where K does not depend on s and the estimate of D is the estimated FD.

4.4. Results

A grand total of 110 FD estimates were analysed statistically. They were obtained for 30 soybean cultivars with 4 individual plants as replicates (alias “POT1”, “POT2”, “POT3”, and “POT4”) per cultivar in general and only 2 or 3 plants for a few cultivars (Table 4.2), providing robust foundation for statistical analysis and ensuring good reliability of findings. While it is acknowledged that this dataset corresponds to an unbalanced completely randomized design, it is important to note that this is the only unbalanced design for which the treatment sample means can readily serve as the least-squares estimators of the treatment means. The objective of this analysis was twofold: assessing the phenotypic variation and validating FD as indicator

of the structural complexity of soybean root systems. The GLM procedure from the SAS software, Version 9.4 for Windows (SAS Institute Inc., Cary, NC, USA) was used for the one-way analysis of variance (ANOVA) and subsequent pairwise comparisons of means among cultivars at the significance level of 5%.

Table 4.2: Estimated FDs of root systems for the 30 experimental soybean cultivars

No.	Soybean Cultivars	POT1		POT2		POT3		POT4		Mean FD	SE
		FD	R^2	FD	R^2	FD	R^2	FD	R^2		
1	4004P4J	1.398	0.998	1.214	0.997	1.0954	0.994	1.442	0.999	1.2873	0.081
2	400524J	1.332	0.997	1.599	0.992	1.5399	0.999	1.453	0.993	1.4811	0.058
3	PS44	1.219	0.982	1.459	0.998	1.3443	0.998	1.251	0.98	1.3182	0.054
4	OAC726-C	1.384	0.996	1.168	0.992	1.3136	0.996	1.328	0.996	1.2985	0.046
5	AC2001	1.358	0.999	1.376	0.983	1.3486	1	1.415	0.981	1.3743	0.015
6	CASINO	1.487	0.999	1.211	0.997	1.223	0.99	1.288	1	1.3024	0.064
7	SASKA					1.2773	0.992	1.29	0.988	1.2835	0.006
8	OAC-WALLACE	1.441	0.999	1.39	1	1.4501	0.998			1.427	0.019
9	505543G			1.498	0.995	1.3161	0.971	1.319	0.995	1.3777	0.06
10	COSTAUD	1.417	0.999	1.431	1	1.3211	0.991			1.3898	0.035
11	MAPLE DONOVAN	1.433	0.999	1.381	0.999	1.5286	0.997	1.443	0.999	1.4464	0.031
12	VENUS	1.409	0.998	1.387	0.999	1.5939	0.997	1.654	0.992	1.5109	0.067
13	OAC7-6C	1.327	0.994	1.356	0.999	1.3388	0.988	1.468	0.973	1.3726	0.032
14	OAC-HAMPION	1.369	0.999	1.372	1	1.3937	1	1.437	0.967	1.393	0.016
15	OAC9-22C	1.607	0.998	1.515	0.999	1.3148	1	1.469	0.998	1.4765	0.061
16	TUNDRA	1.57	0.999	1.319	0.988					1.4446	0.126
17	OAC1-26C	1.61	0.993	1.473	1	1.4725	0.99	1.614	0.997	1.5424	0.04
18	WOODSTOCK	1.257	0.963	1.533	1	1.3863	0.998	1.444	0.999	1.4051	0.058
19	DUNDAS	1.408	0.998	1.512	1	1.4774	0.988	1.389	0.987	1.4466	0.029
20	OAC8-21C	1.429	0.978	1.454	0.998	1.3414	0.997	1.366	0.99	1.3975	0.026
21	ACGLENGARRY	1.376	1	1.347	0.991	1.3188	0.999	1.314	1	1.3391	0.014
22	McCALL					1.5308	1	1.281	0.992	1.406	0.125
23	GENTLEMAN	1.332	1	1.423	0.998	1.5002	0.997	1.546	0.998	1.4502	0.047
24	S03-W4	1.616	0.997	1.59	0.997	1.574	0.999	1.338	0.997	1.5294	0.064
25	OAC-OXFORD	1.489	0.992	1.469	1	1.3587	0.999	1.35	0.996	1.4166	0.036
26	OAC-KENT	1.541	0.983	1.368	0.993	1.5462	0.997	1.196	0.995	1.4127	0.083
27	OAC7-4C			1.341	0.997	1.5543	0.998	1.261	0.998	1.3856	0.087
28	WALTON	1.263	0.994	1.291	0.99	1.3188	0.997	1.433	0.984	1.3265	0.037
29	GAILLARD	1.417	0.999	1.413	0.998	1.462	0.992	1.519	0.999	1.4527	0.025
30	DRAYTON	1.519	0.999	1.5	0.999	1.3497	0.999	1.383	0.995	1.4378	0.042

One-way ANOVA:

With an observed value of 1.82 for the ANOVA F-test statistic and an associated p-value of $0.0192 < 0.05$, there are statistically significant differences in FD estimates among the 30 soybean cultivars. This result suggests that at least two soybean cultivars exhibit different levels of root system complexity. The R^2 value of 0.397 for the model goodness-of-fit indicates that 39.7% of the total variation in FD estimates can be attributed to differences among cultivars, highlighting that the cultivar significantly impacts the root system FD but leaving a nonetheless important portion (60.3%) for variability among individual plants from the same cultivar and the experimental error. Two other statistics worth reporting are: an overall sample mean FD value of 1.406 and a coefficient of variation of 7.09%, indicating a low variability in FD values relative to their mean. The distribution of FD estimates across the 30 soybean cultivars is shown in Figure 4.1. It provides a first comparative view, illustrating how FD values are spread among and within cultivars. By visualising the distribution of FD, this figure helps identify patterns in root system complexity, highlighting cultivars with higher FD values that may indicate better adaptability to environmental stresses. Cultivars such as 17 (OAC1-26C), with mean FDs around 1.5, have a more complex RSA that is likely better suited to adapt to drought or poor soil conditions. Conversely, cultivars with lower mean FDs around 1.3, such as 21 (ACGLENGARRY), possess simpler root systems that may limit their adaptability to challenging environmental stresses.

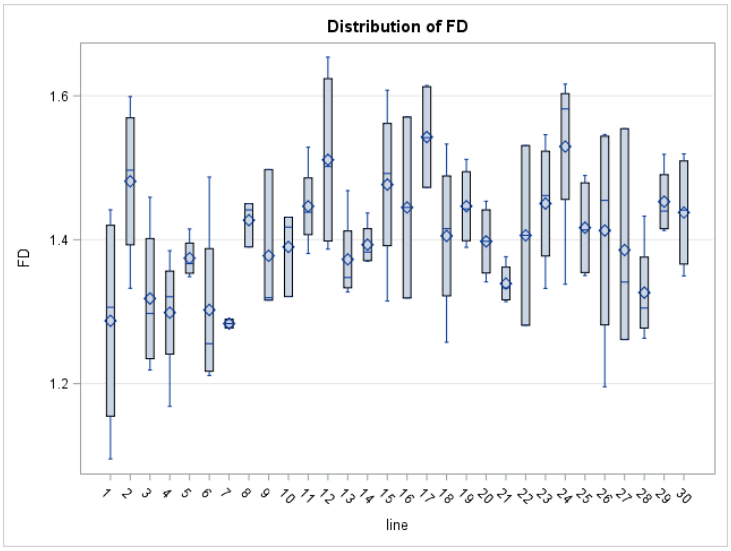

Figure 4.1: Distribution of FD values and mean by cultivar

Pairwise Comparisons:

Following the results of the one-way ANOVA, the procedure of multiple pairwise comparisons of means based on the Least Significant Difference (LSD) was performed to identify pairs of soybean cultivars with statistically significant differences in root system FD at the 0.05 level values. Several comparisons showed significant differences, highlighting distinct degrees of root system complexity between cultivars, the cultivars with significant pairwise differences are reported in Table D1. For example, cultivars 17 (OAC1-26C) and 14 (OAC-CHAMPION) showed a significant difference in FD mean of 0.14942 (95% confidence interval: [0.00911, 0.28974]), indicating a notable difference in root system complexity. Examples of cultivars exhibiting significant differences in FD mean values with several other soybean cultivars include: 12 (VENUS), 2 (400524J), 15 (OAC9-22C), 29 (GAILLARD), and 23 (GENTLEMAN), further emphasizing the diversity in root system complexity within the population. These findings support the use of FD as a reliable metric for assessing root system complexity and provide a valuable foundation for future research.

Visual Representation:

Results of the pairwise comparisons of FD means among the 30 soybean cultivars are plotted in Figure 4.2, where the dashed diagonal line represents equality in FD means, the red line segments identify the non-significant ($p \geq 0.05$) pairwise comparisons, and the blue line segments highlight the pairs of cultivars with significant ($p < 0.05$) differences between FD means. Notably, among the 30*29/2 = 435 comparisons of 2 different soybean cultivars, 57 produced a statistically significant result at 5%, and among them, cultivar 17 (OAC1-26C) is involved 14 times, and cultivar 24 (S03-W4), 10 times. It must be noted that in Table D1, each significant pair of cultivars is reported twice (e.g., 24-1 and 1-24).

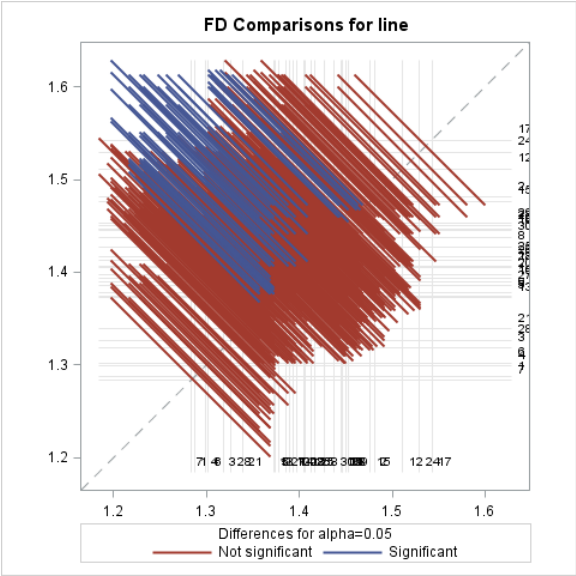

Figure 4.2: Pairwise Comparisons of FD Means between Cultivars

4.5. Discussion

This study aimed to enhance the understanding of soybean RSA in a growing medium that mimics a natural environment, using CT scanning technology and fractal analysis based on FDs estimated from reconstructed 3D images of root systems. The data collected, together with the results of our image analysis and statistical analysis, revealed substantial variability in root

system complexity among the 30 experimental soybean cultivars, thus highlighting the diversity in RSA. The variability that we observed aligns with and refines the variability reported in previous studies that followed a different approach (e.g., in 2D without a CT scanner) but already underscored the genetic diversity of soybean root systems. Such diversity is crucial for breeding programs aimed at developing cultivars with improved root systems for better nutrient and water uptake, especially in the context of climate change. For instance, Lynch (2022) and Freschet et al. (2021) highlighted the importance of root diversity in improving crop performance under varying environmental conditions. Developmental plasticity plays a crucial role in this variability, allowing plants to adapt to various environmental conditions. This adaptability is essential for survival in unpredictable environments.

Roots can alter their growth direction and elongation rate in response to soil moisture gradients, a phenomenon known as “hydrotropism”. Unlike gravitropism which directs root growth downward, hydrotropism directs roots towards higher moisture levels(Dinneny, 2019; Gul et al., 2023; Watanabe et al., 2020). Studies on Arabidopsis have shown that hydrotropism can override gravitropism, with roots growing preferentially towards environments with higher relative water potential. Genes essential for a hydrotropic response have been identified by mutant screening, revealing the genetic basis of this adaptability (Cassab et al., 2013; Dietrich, 2018; Mao et al., 2022). Moreover, it was noted by Bengough et al. (2016); Dietrich (2018) and Ruiz et al. (2015), that compacted soil layers can create physical barriers that roots must navigate through.

During the experiment, a peculiar root growth pattern was observed in some plants, characterised by an initial downward growth, an upward turn, and then a resumption of downward growth, forming a “crooked J-shape”. The upward turn in crooked J-shaped roots might indicate an encounter with a compacted soil layer, prompting the roots to redirect their

growth path to find a less resistant route. This unusual root morphology could also be attributed to hydrotropism. Due to the presence of a non-uniform water gradient in some pots, these roots may have altered their growth direction to optimise water uptake.

Seed age also has the potential to impact root morphology. Older accessions may exhibit altered root growth patterns due to reduced vigour and potency of the cotyledons (Ebone et al., 2020; Wang et al., 2023). The cotyledons' nutrient supply is crucial for early root development, and less vigorous cotyledons could influence the root's ability to penetrate the soil. This hypothesis aligns with findings that older seeds often produce seedlings with less robust root systems, affecting their overall growth and development. It may be what happened to the 10 soybean seedlings for which the root systems, too poorly developed, were finally discarded from the fractal analysis.

The combination of CT scanning technology and fractal dimension (FD) as a metric provides a non-invasive, precise procedure for evaluating root system complexity, offering a robust framework for 3D phenotyping. The insights gained from this study have important implications for breeding programs and agricultural practices. As a measure of root system architecture (RSA) complexity, FD encompasses various root variables, including angles, curvatures, distances between branching nodes, and both total and individual root lengths. Although the exact function linking FD with these root variables is not fully understood, it is reasonable to assume that some root traits may correlate positively with FD, while some others negatively and the remaining ones not all. When the majority of FD-root trait relationships are positive, it is statistically expected that the variance of FD would increase as the overall variability rises. Without the variance aspect, this reasoning was initially applied in studies of above-ground branching patterns (Foroutan-pour et al., 2001).

While 60.3% of the variation unrelated to differences among cultivars might seem substantial, it must be noted that the error variance estimate is only 0.0099, or 1%. Very interestingly, the

FD estimates obtained in this study show statistically significant differences between cultivars, along with an important variability in root system complexity among individual plants within the same cultivar. Based on the mean FD values (Table 4.2), it can be hypothesized that the two soybean cultivars with the highest FD means (OAC1-26C and S03-W4) are likely to perform better under environmental stresses, whereas the cultivars with the lowest FD means (4004P4J and SASKA) may exhibit poorer performance under such conditions. Understanding the factors influencing RSA could thus aid in selecting soybean cultivars with superior root traits, leading to improved water and nutrient uptake and, consequently, enhanced crop performance in the field. Eventually, field studies incorporating a variety of soil profiles and environmental stresses would validate these findings, obtained under partially controlled growing conditions, and enhance their application to real-world agricultural settings.

4.6. Conclusion

This study successfully demonstrated the utility of a 3D phenotyping framework in assessing phenotypic variation in RSA among soybean cultivars at an early stage of development. The significant differences found in FD mean, using ANOVA and multiple pairwise comparisons, validate its use as an indicator of root system complexity, providing valuable insights for developing climate-resilient soybean cultivars. This work and the results obtained constitute an important advancement in methodology towards a comprehensive analysis of RSA traits. The transition from 2D to 3D RSA phenotyping represents a key step in the overarching goal of promoting agricultural sustainability through enhanced resource-use efficiency and stress tolerance, here, in soybean.

4.7. Acknowledgements

This research was supported by the Fonds de recherche du Québec – Nature et technologies (FRQNT), through a "Projet de recherche en équipe" grant to F. Belzile and P. Dutilleul. The CT scanning work would not have been possible without the support of the Canada Foundation for Innovation (CFI) through the Geitmann CFI 9 grant, which provided the modern macro-CT scanning equipment as part of the Eastern Canadian Plant Phenotyping Platform (ECP3). We are grateful to Miss Mounawarath Assani for her assistance in growing plants and conducting germination tests at Université Laval.

4.8. References

Adeleke, E., Millas, R., McNeal, W., Faris, J., & Taheri, A. (2019). Assessing root system architecture of wheat seedlings using A high-throughput root phenotyping system. *BioRxiv*, 677955.

Adu, M. O., Chatot, A., Wiesel, L., Bennett, M. J., Broadley, M. R., White, P. J., & Dupuy, L. X. (2014). A scanner system for high-resolution quantification of variation in root growth dynamics of Brassica rapa genotypes. *Journal of Experimental Botany*, *65*(8), 2039-2048.

Atkinson, J. A., Pound, M. P., Bennett, M. J., & Wells, D. M. (2019). Uncovering the hidden half of plants using new advances in root phenotyping. *Current opinion in biotechnology*, *55*, 1-8.

Ayalew, H., Liu, H., Börner, A., Kobiljski, B., Liu, C., & Yan, G. (2018). Genome-wide association mapping of major root length QTLs under PEG induced water stress in wheat. *Frontiers in Plant Science*, *9*, 1759.

Bengough, A. G., Loades, K., & McKenzie, B. M. (2016). Root hairs aid soil penetration by anchoring the root surface to pore walls. *Journal of Experimental Botany*, *67*(4), 1071-1078.

Brevedan, R., & Egli, D. (2003). Short periods of water stress during seed filling, leaf senescence, and yield of soybean. *Crop Science*, *43*(6), 2083-2088.

Cassab, G. I., Eapen, D., & Campos, M. E. (2013). Root hydrotropism: an update. *American journal of botany*, *100*(1), 14-24.

Dietrich, D. (2018). Hydrotropism: how roots search for water. *Journal of Experimental Botany*, *69*(11), 2759-2771.

Dinneny, J. R. (2019). Developmental Responses to Water and Salinity in Root Systems. *Annual Review of Cell and Developmental Biology*, *35*(1), 239-257. https://doi.org/10.1146/annurev-cellbio-100617-062949

Ebone, L. A., Caverzan, A., Tagliari, A., Chiomento, J. L. T., Silveira, D. C., & Chavarria, G. (2020). Soybean Seed Vigor: Uniformity and Growth as Key Factors to Improve Yield. *Agronomy*, *10*(4), 545. https://www.mdpi.com/2073-4395/10/4/545

Foroutan-pour, K., Dutilleul, P., & Smith, D. L. (1999 a). Soybean Canopy Development as Affected by Population Density and Intercropping with Com: Fractal Analysis in Comparison with Other Quantitative Approaches. *Crop Science*, *39*(6), 1784-1791.

Foroutan-pour, K., Dutilleul, P., & Smith, D. L. (1999 b). Advances in the implementation of the box-counting method of fractal dimension estimation. *Applied mathematics and computation*, *105*(2-3), 195-210.

Freschet, G. T., Roumet, C., Comas, L. H., Weemstra, M., Bengough, A. G., Rewald, B., Bardgett, R. D., De Deyn, G. B., Johnson, D., & Klimešová, J. (2021). Root traits as drivers of plant and ecosystem functioning: current understanding, pitfalls and future research needs. *New phytologist*, *232*(3), 1123-1158.

Gul, M. U., Paul, A., & Chehri, A. (2023). Hydrotropism: understanding the impact of water on plant movement and adaptation. *Water*, *15*(3), 567.

Han, L., Dutilleul, P., Prasher, S. O., Beaulieu, C., & Smith, D. L. (2008). Assessment of Common Scab-Inducing Pathogen Effects on Potato Underground Organs Via Computed Tomography Scanning. *Phytopathology*, *98*(10), 1118.

Han, L., Dutilleul, P., Prasher, S. O., Beaulieu, C., & Smith, D. L. (2009). Assessment of Density Effects of the Common Scab-Inducing Pathogen on the Seed and Peripheral Organs of Potato During Growth Using Computed Tomography Scanning Data. *Transactions of the ASABE*, *52*(1), 305-311. https://doi.org/10.13031/2013.25924

Hargreaves, C. E., Gregory, P. J., & Bengough, A. G. (2009). Measuring root traits in barley (Hordeum vulgare ssp. vulgare and ssp. spontaneum) seedlings using gel chambers, soil sacs and X-ray microtomography. *Plant and soil*, *316*, 285-297.

Hund, A., Trachsel, S., & Stamp, P. (2009). Growth of axile and lateral roots of maize: I development of a phenotying platform. *Plant and soil*, *325*, 335-349.

Islam, I., Adam, Z., & Islam, S. (2019). Soybean (Glycine Max): alternative sources of human nutrition and bioenergy for the 21st century. *Am. J. Food Sci. Technol*, *7*, 1-6.

Kuijken, R. C., van Eeuwijk, F. A., Marcelis, L. F., & Bouwmeester, H. J. (2015). Root phenotyping: from component trait in the lab to breeding. *Journal of Experimental Botany*, *66*(18), 5389-5401.

Lakhiar, I. A., Jianmin, G., Syed, T. N., Chandio, F. A., Buttar, N. A., & Qureshi, W. A. (2018). Monitoring and control systems in agriculture using intelligent sensor techniques: A review of the aeroponic system. *Journal of Sensors*, *2018*, 1-18.

Lontoc-Roy, M., Dutilleul, P., Prasher, S. O., Han, L., Brouillet, T., & Smith, D. L. (2006). Advances in the acquisition and analysis of CT scan data to isolate a crop root system from the soil medium and quantify root system complexity in 3-D space. *Geoderma*, *137*(1-2), 231-241.

Lynch, J. P. (2022). Harnessing root architecture to address global challenges. *The Plant Journal*, *109*(2), 415-431.

Mandelbrot, B. B. (1982). *The fractal geometry of nature* (Vol. 1). WH freeman New York.

Mao, B., Takahashi, H., Takahashi, H., & Fujii, N. (2022). Diversity of root hydrotropism among natural variants of Arabidopsis thaliana. *Journal of Plant Research*, *135*(6), 799-808.

Mooney, S. J., Pridmore, T. P., Helliwell, J., & Bennett, M. J. (2012). Developing X-ray Computed Tomography to non-invasively image 3-D root systems architecture in soil. *Plant and soil*, *352*(1-2), 1-22. https://doi.org/10.1007/s11104-011-1039-9

Morrison, M., McLaughlin, N., Cober, E., & Butler, G. (2006). When is short-season soybean most susceptible to water stress? *Canadian journal of plant science*, *86*(Special Issue), 1327-1331.

Osvald, J., Petrovic, N., & Demsar, J. (2001). Sugar and organic acid content of tomato fruits (Lycopersicon lycopersicum Mill.) grown on aeroponics at different plant density. *Acta Alimentaria*, *30*(1), 53-61.

Rogers, E. D., Monaenkova, D., Mijar, M., Nori, A., Goldman, D. I., & Benfey, P. N. (2016). X-Ray Computed Tomography Reveals the Response of Root System Architecture to Soil Texture *Plant physiology*, *171*(3), 2028-2040. https://doi.org/10.1104/pp.16.00397

Ruiz, S., Or, D., & Schymanski, S. J. (2015). Soil Penetration by Earthworms and Plant Roots—Mechanical Energetics of Bioturbation of Compacted Soils. *PloS one*, *10*(6), e0128914. https://doi.org/10.1371/journal.pone.0128914

Sanghera, P., Belzile, F., Seck, W., & Dutilleul, P. (2023). Cluster Analysis of 137 Soybean Lines Based on Root System Architecture Traits Measured in Rhizoboxes.

Seck, W., Torkamaneh, D., & Belzile, F. (2020). Comprehensive genome-wide association analysis reveals the genetic basis of root system architecture in soybean. *Frontiers in Plant Science*, *11*, 590740.

Selvaraj, M. G., Montoya-P, M. E., Atanbori, J., French, A. P., & Pridmore, T. (2019). A low-cost aeroponic phenotyping system for storage root development: unravelling the below-ground secrets of cassava (*Manihot esculenta*). *Plant Methods*, *15*, 1-13.

Singh, I., Pathak, J., Mahajan, M., Nehte, D., & Singh, L. (2018). Enhancing soybean yield through improved production technology under frontline demonstration in Madhya Pradesh and Maharashtra. *Journal of Community Mobilization and Sustainable Development*, *13*(3), 442-446.

Subramanian, S., Han, L., Dutilleul, P., & Smith, D. L. (2015). Computed tomography scanning can monitor the effects of soil medium on root system development: an example of salt stress in corn. *Frontiers in Plant Science*, *6*. https://doi.org/10.3389/fpls.2015.00256

Trachsel, S., Kaeppler, S. M., Brown, K. M., & Lynch, J. P. (2011). Shovelomics: high throughput phenotyping of maize (*Zea mays* L.) root architecture in the field. *Plant and soil*, *341*, 75-87.

Wang, Y., Zhou, E., Yao, M., Xue, D., Zhao, N., Zhou, Y., Li, B., Wang, K., Miao, Y., Gu, C., Wang, X., & Wei, L. (2023). PEG-6000 Priming Improves Aged Soybean Seed Vigor via Carbon Metabolism, ROS Scavenging, Hormone Signaling, and Lignin Synthesis Regulation. *Agronomy*, *13*(12), 3021. https://www.mdpi.com/2073-4395/13/12/3021

Watanabe, Y., Kabuki, T., Kakehashi, T., Kano-Nakata, M., Mitsuya, S., & Yamauchi, A. (2020). Morphological and histological differences among three types of component roots and their differential contribution to water uptake in the rice root system. *Plant Production Science*, *23*(2), 191-201.

Chapter 5: General Discussion

This study aimed to develop an appropriate 3D phenotyping framework for soybean root system architecture (RSA) and establish fractal dimension (FD) as a quantitative indicator of root system complexity. Conducted within the broader context of sustainable agriculture, this research harnessed state-of-the-art imaging technologies alongside rigorous statistical methods to tackle significant challenges in soybean cultivation. This general discussion provides a comprehensive synthesis of the key findings, critically evaluates the employed methodologies, and explores the broader implications of the results within the framework of existing literature, also proposing future research directions.

In Chapter 3, a dataset on the RSA of 137 soybean cultivars grown in a 2D study, composed of traits such as root lengths, numbers, depth, diameter, and surface area, was analysed statistically after a significant genetic diversity had been formerly highlighted in it; such a diversity is essential for breeding programs aimed at improving soybean resilience and yield.

To analyse the dataset, the multivariate statistical method of Principal Component Analysis (PCA) was performed to reduce the dimensionality of the data table while retaining most of the variability contained in it. With biplots of a small number of principal components, the PCA provided a clear understanding of the relationships among the RSA traits. The visualisation of principal components made it evident how certain traits grouped together and how they influenced the overall RSA.

Following PCA, cluster analysis was applied to group the 137 soybean cultivars into 30 distinct clusters, using algorithms to classify cultivars into clusters where the members are more similar

to each other than to members of other clusters; similarity was based on the Euclidean distance in the multi-dimensional space of the RSA traits.

From each of the 30 clusters, one representative soybean cultivar was chosen for its proximity to the centre of the cluster, for study in a 3D setup. This procedure ensured that the diversity of RSA traits observed in the former 2D study was captured and would be transferred to the next level of analysis.

Available seeds from the representative cultivars were subjected to germination tests, before studying the RSA of the soybean seedlings in a more complex environment. This step was crucial because the seeds were going to be sown in soil (sand), whereas already germinated seeds had been transplanted in an artificial medium (vermiculite) in the 2D study. Thus, the genetic diversity expressed in the 3D setup was going to incorporate this important difference, which makes the growing medium in the 3D setup closer to that in the field.

Chapter 4 makes the transition from 2D to 3D RSA phenotyping happen for 30 soybean cultivars, one per cluster identified in Chapter 3. X-ray computed tomography (CT) scanning was instrumental in the advancement to 3D
RSA phenotyping, as this technology allows for non-destructive and high-resolution imaging of soybean root systems grown in soil, providing a realistic view *in situ* of their structure in 3D. Aspects of the RSA that are not discernible in 2D images were thus revealed, including the 3D spatial distribution of roots, the density of root networks, and intricate root branching patterns.

One of the significant contributions of this chapter concerns the fractal dimension as a measure of root system complexity. The FD is a mathematical metric that quantifies the complexity (tortuosity, branching) of a structure. In the context of RSA, a higher FD indicates a more complex root system, which is often associated with better adaptability to environmental stresses.

The experimental results reported in Chapter 4 provide evidence in support of FD being a reliable and meaningful indicator of complexity for soybean root systems at an early stage of development. By analysing the 3D images reconstructed from CT scanning data, FD estimates were obtained, one per plant, and the one-way analysis of variance performed on FD estimates revealed soybean cultivars with significantly different root system complexity. Thus, the FD metric provides a sound basis for a practical assessment of differences in the structural complexity of root systems.

The advancements presented in Chapter 4 lay a strong foundation for future research in plant phenotyping, emphasizing the importance of integrating advanced imaging technologies, mathematical metrics and statistical analyses with large sample sizes to address the challenges of sustainable agriculture.

As part of the innovative 3D RSA phenotyping framework presented in this thesis, the ability to CT scan more than 100 individual plants in one day represents a significant advancement in the field of plant phenotyping. This high-throughput capability is facilitated by a modern tool like the Canon Aquilion Prime SP macro-CT scanner, which is part of the Eastern Canadian Plant Phenotyping Platform (ECP3). This CT scanner provides precision and efficiency, but its software, designed for medical applications, had to be replaced by programs written in

MATLAB (The MathWorks Inc.) for imaging plant root systems. The combination of advanced imaging technology and a sophisticated programming language enables the generation of detailed 3D models that quantify RSA, providing invaluable insight into the spatial distribution of roots in soil. This advancement addresses the inherent complexities of RSA, such as overlapping roots, curves, and bends, which often exceed the capabilities of conventional imaging techniques.

This comprehensive approach ensures a reliable analysis of the RSA, which will eventually aid breeders in selecting soybean cultivars with desirable root traits. Such soybean cultivars should have enhanced resilience to abiotic stresses, such as drought and poor soil fertility, contributing to sustainable agricultural practices and crop improvement efforts.

CT scanning technology is non-destructive and non-invasive, thus preserving the natural soil environment and root-soil interactions. This is key for maintaining realistic conditions for root growth studies, whereas artificial growing media, especially in 2D studies, likely do not reproduce field conditions. Plant CT scanning of soil-filled pots provides a more accurate evaluation of root behaviour. This realistic approach ensures an effective transition from laboratory findings to field applications, maintaining relevance to actual agricultural practices. By integrating soil environments in high-resolution imaging studies, this framework achieves a balance between conditions controlled up to a certain level and realistic 3D root system modelling, enhancing the agronomic applicability of RSA phenotyping research.

Chapter 6: General Conclusion

This thesis provides a robust 3D phenotyping framework for understanding and quantifying the complexity of root system architecture (RSA) in soybean at an early stage of development. Through the integration of advanced imaging technologies, statistical analyses, and metrics such as fractal dimension (FD), the research has addressed critical challenges in soybean cultivation, particularly in the context of sustainable agriculture and climate change.

Principal Component Analysis and cluster analysis were successfully used to identify representative soybean cultivars based on multiple RSA traits, ensuring that subsequent detailed phenotyping was both manageable and representative of the broad, genetic and phenotypic diversity within the soybean population. The transition from 2D to 3D RSA phenotyping, facilitated by X-ray computed tomography (CT) scanning, provided high-resolution, non-destructive imaging that revealed structural details of root systems that are often missed in traditional 2D analyses. The results established FD as a reliable measure of root system complexity for the comparison and assessment of differences in RSA among soybean cultivars. FD offers a mathematical metric to quantify the structural complexity of root systems, providing breeders with a new tool for selecting root traits associated with improved water and nutrient uptake. This is particularly relevant for developing soybean varieties better adapted to varying environmental conditions, thus contributing to the goals of sustainable agriculture.

Any research is not without limitations. We are not aware of the existence of a macro-CT scanner that could be brought to and be used in an agricultural field. The environment of pot-grown plants does not reproduce the variability and heterogeneity of field conditions, emphasising the need for validation of our findings in field conditions. Therefore, our results

will soon be compared with results obtained by a collaborator on the FRQNT “Projet de recherche en équipe”, in a series of field experiments conducted at Agriculture and Agri-Food Canada.

Future research should focus on several key areas to build on the findings of this thesis. More field trials are essential to validate our results under diverse environmental conditions. Integrating genomic data with RSA phenotyping could uncover the genetic determinants of root traits and their interactions with environmental factors, providing deeper insights into the genetic basis of root complexity. Extending the methodologies developed in this study to other crop species could enhance the generalisation and applicability of the findings, benefiting a wider range of agricultural practices. Developing cost-effective and scalable imaging technologies for root systems, and not only for leaf canopies, will be crucial for facilitating the broader adoption of advanced phenotyping methods in breeding programs.

In conclusion, this thesis has laid a solid foundation for advancing our understanding of the RSA in soybean. The innovative use of 3D imaging and fractal analysis, in larger numbers of plants than ever before at the CT Scanning Laboratory for agricultural and environmental research, has provided new insights into root complexity, offering valuable tools for breeding resilient soybean varieties. Despite the remaining challenges, the methodologies and findings from this research have significant implications for sustainable agriculture and the ongoing efforts to enhance global food security.

Bibliography

Adeleke, E., Millas, R., McNeal, W., Faris, J., & Taheri, A. (2019). Assessing root system architecture of wheat seedlings using A high-throughput root phenotyping system. *BioRxiv*, 677955.

Adu, M. O., Chatot, A., Wiesel, L., Bennett, M. J., Broadley, M. R., White, P. J., & Dupuy, L. X. (2014). A scanner system for high-resolution quantification of variation in root growth dynamics of Brassica rapa genotypes. *Journal of Experimental Botany*, *65*(8), 2039-2048.

Alexandersson, E., Jacobson, D., Vivier, M. A., Weckwerth, W., & Andreasson, E. (2014). Field-omics—understanding large-scale molecular data from field crops. *Frontiers in Plant Science*, *5*, 286.

Atkinson, J. A., Pound, M. P., Bennett, M. J., & Wells, D. M. (2019). Uncovering the hidden half of plants using new advances in root phenotyping. *Current opinion in biotechnology*, *55*, 1-8.

Aulakh, M., Wassmann, R., Bueno, C., Kreuzwieser, J., & Rennenberg, H. (2001). Characterization of root exudates at different growth stages of ten rice (*Oryza sativa* L.) cultivars. *Plant biology*, *3*(02), 139-148.

Ayalew, H., Liu, H., Börner, A., Kobiljski, B., Liu, C., & Yan, G. (2018). Genome-wide association mapping of major root length QTLs under PEG induced water stress in wheat. *Frontiers in Plant Science*, *9*, 1759.

Aylmore, L. (1993). Use of computer-assisted tomography in studying water movement around plant roots. *Advances in Agronomy*, *49*, 1-54.

Bengough, A. G., Loades, K., & McKenzie, B. M. (2016). Root hairs aid soil penetration by anchoring the root surface to pore walls. *Journal of Experimental Botany*, *67*(4), 1071-1078.

Bingham, I. J., Bengough, A. G., & Rees, R. M. (2010). Soil compaction–N interactions in barley: Root growth and tissue composition. *Soil and Tillage Research*, *106*(2), 241-246.

Bouteillé, M., Rolland, G., Balsera, C., Loudet, O., & Muller, B. (2012). Disentangling the intertwined genetic bases of root and shoot growth in Arabidopsis. *PloS one*, *7*(2), e32319.

Bradshaw, A. D. (1965). Evolutionary significance of phenotypic plasticity in plants. *Advances in genetics*, *13*, 115-155.

Brevedan, R., & Egli, D. (2003). Short periods of water stress during seed filling, leaf senescence, and yield of soybean. *Crop Science*, *43*(6), 2083-2088.

Bucksch, A., Burridge, J., York, L. M., Das, A., Nord, E., Weitz, J. S., & Lynch, J. P. (2014). Image-based high-throughput field phenotyping of crop roots. *Plant physiology*, *166*(2), 470-486.

Bueno, R. D., Borges, L. L., God, P. I. G., Piovesan, N. D., Teixeira, A. I., Cruz, C. D., & BARROS, E. G. (2018). Quantification of anti-nutritional factors and their correlations with protein and oil in soybeans. *Anais da Academia Brasileira de Ciências*, *90*, 205-217.

Burton, A. L., Williams, M., Lynch, J. P., & Brown, K. M. (2012). RootScan: software for high-throughput analysis of root anatomical traits. *Plant and soil*, *357*, 189-203.

Bylesjö, M., Eriksson, D., Kusano, M., Moritz, T., & Trygg, J. (2007). Data integration in plant biology: the O2PLS method for combined modeling of transcript and metabolite data. *The Plant Journal*, *52*(6), 1181-1191.

Canada, S. (2022). https://www150.statcan.gc.ca/n1/daily-quotidien/221202/dq221202b-eng.htm
Canarini, A., Kaiser, C., Merchant, A., Richter, A., & Wanek, W. (2019). Root Exudation of Primary Metabolites: Mechanisms and Their Roles in Plant Responses to Environmental Stimuli. *Frontiers in Plant Science*, *10*. https://doi.org/10.3389/fpls.2019.00157
Casero, P., Casimiro, I., & Lloret, P. (1995). Lateral root initiation by asymmetrical transverse divisions of pericycle cells in four plant species: Raphanus sativus, Helianthus annuus, Zea mays, and Daucus carota. *Protoplasma*, *188*, 49-58.
Cassab, G. I., Eapen, D., & Campos, M. E. (2013). Root hydrotropism: an update. *American journal of botany*, *100*(1), 14-24.
Chen, Y. L., Dunbabin, V. M., Diggle, A. J., Siddique, K. H., & Rengel, Z. (2011). Development of a novel semi-hydroponic phenotyping system for studying root architecture. *Functional Plant Biology*, *38*(5), 355-363.
Chen, Y. L., Palta, J., Clements, J., Buirchell, B., Siddique, K. H., & Rengel, Z. (2014). Root architecture alteration of narrow-leafed lupin and wheat in response to soil compaction. *Field Crops Research*, *165*, 61-70.
Clark, R. T., Famoso, A. N., Zhao, K., Shaff, J. E., Craft, E. J., Bustamante, C. D., McCouch, S. R., Aneshansley, D. J., & Kochian, L. V. (2013). High-throughput two-dimensional root system phenotyping platform facilitates genetic analysis of root growth and development. *Plant, cell & environment*, *36*(2), 454-466.
Clark, R. T., MacCurdy, R. B., Jung, J. K., Shaff, J. E., McCouch, S. R., Aneshansley, D. J., & Kochian, L. V. (2011). Three-dimensional root phenotyping with a novel imaging and software platform. *Plant physiology*, *156*(2), 455-465.
Colombi, T., & Walter, A. (2015). Root responses of triticale and soybean to soil compaction in the field are reproducible under controlled conditions. *Functional Plant Biology*, *43*(2), 114-128.
Correa, J., Postma, J. A., Watt, M., & Wojciechowski, T. (2019). Soil compaction and the architectural plasticity of root systems. *Journal of Experimental Botany*, *70*(21), 6019-6034. https://doi.org/10.1093/jxb/erz383
Crestana, S., Cesareo, R., & Mascarenhas, S. (1986). Using a computed tomography miniscanner in soil science. *Soil Science*, *142*(1), 56.
Dayan, F. E., Watson, S. B., & Nanayakkara, N. D. (2007). Biosynthesis of lipid resorcinols and benzoquinones in isolated secretory plant root hairs. *Journal of Experimental Botany*, *58*(12), 3263-3272.
Des Marais, D. L., Hernandez, K. M., & Juenger, T. E. (2013). Genotype-by-Environment Interaction and Plasticity: Exploring Genomic Responses of Plants to the Abiotic Environment. *Annual Review of Ecology, Evolution, and Systematics*, *44*(1), 5-29. https://doi.org/10.1146/annurev-ecolsys-110512-135806
Dietrich, D. (2018). Hydrotropism: how roots search for water. *Journal of Experimental Botany*, *69*(11), 2759-2771.
Dinneny, J. R. (2019). Developmental Responses to Water and Salinity in Root Systems. *Annual Review of Cell and Developmental Biology*, *35*(1), 239-257. https://doi.org/10.1146/annurev-cellbio-100617-062949
Douarre, C., Schielein, R., Frindel, C., Gerth, S., & Rousseau, D. (2016). Deep learning based root-soil segmentation from X-ray tomography images. *BioRxiv*, 071662.
Dresbøll, D. B., Thorup-Kristensen, K., McKenzie, B. M., Dupuy, L. X., & Bengough, A. G. (2013). Timelapse scanning reveals spatial variation in tomato *(Solanum lycopersicum* L.) root elongation rates during partial waterlogging. *Plant and soil*, *369*, 467-477.

Dunbabin, V., & Postma, J. (2013). Schnepf Aet al. 2013. Modelling root-soil interactions using three-dimensional models of root growth, architecture and function. *Plant and Soil372*, 93-124.
Dutilleul, P., Han, L., & Smith, D. L. (2008). Plant light interception can be explained via computed tomography scanning: Demonstration with pyramidal cedar (*Thuja occidentalis, Fastigiata*). *Annals of Botany*, *101*(1), 19-23.
Dutilleul, P., Lontoc-Roy, M., & Prasher, S. O. (2005). Branching out with a CT scanner. *Trends in plant science*, *10*(9), 411-412.
Eavis, B. (1972). Soil physical conditions affecting seedling root growth: I. Mechanical impedance, aeration and moisture availability as influenced by bulk density and moisture levels in a sandy loam soil. *Plant and soil*, *36*, 613-622.
Ebone, L. A., Caverzan, A., Tagliari, A., Chiomento, J. L. T., Silveira, D. C., & Chavarria, G. (2020). Soybean Seed Vigor: Uniformity and Growth as Key Factors to Improve Yield. *Agronomy*, *10*(4), 545. https://www.mdpi.com/2073-4395/10/4/545
Falk, K. G., Jubery, T. Z., Mirnezami, S. V., Parmley, K. A., Sarkar, S., Singh, A., Ganapathysubramanian, B., & Singh, A. K. (2020). Computer vision and machine learning enabled soybean root phenotyping pipeline. *Plant Methods*, *16*, 1-19.
Fan, G., Liang, H., Zhao, Y., & Li, Y. (2022). Automatic reconstruction of three-dimensional root system architecture based on ground penetrating radar. *Computers and Electronics in Agriculture*, *197*, 106969.
Fitter, A. (1987). An architectural approach to the comparative ecology of plant root systems. *New phytologist*, *106*, 61-77.
Foroutan-pour, K., Dutilleul, P., & Smith, D. L. (1999 a). Soybean Canopy Development as Affected by Population Density and Intercropping with Com: Fractal Analysis in Comparison with Other Quantitative Approaches. *Crop Science*, *39*(6), 1784-1791.
Foroutan-pour, K., Dutilleul, P., & Smith, D. L. (1999 b). Advances in the implementation of the box-counting method of fractal dimension estimation. *Applied mathematics and computation*, *105*(2-3), 195-210.
Foroutan-pour, K., Dutilleul, P., & Smith, D. L. (2001). Inclusion of the Fractal Dimension of Leafless Plant Structure in the Beer-Lambert Law. *Agronomy Journal*, *93*(2), 333-338. https://doi.org/10.2134/agronj2001.932333x
Freschet, G. T., Roumet, C., Comas, L. H., Weemstra, M., Bengough, A. G., Rewald, B., Bardgett, R. D., De Deyn, G. B., Johnson, D., & Klimešová, J. (2021). Root traits as drivers of plant and ecosystem functioning: current understanding, pitfalls and future research needs. *New phytologist*, *232*(3), 1123-1158.
Fried, H. G., Narayanan, S., & Fallen, B. (2019). Evaluation of soybean [*Glycine max* (L.) Merr.] genotypes for yield, water use efficiency, and root traits. *PloS one*, *14*(2), e0212700.
Fukaki, H., & Tasaka, M. (2009). Hormone interactions during lateral root formation. *Plant molecular biology*, *69*, 437-449.
Furbank, R. T., & Tester, M. (2011). Phenomics–technologies to relieve the phenotyping bottleneck. *Trends in plant science*, *16*(12), 635-644.
Gai, J., Liu, Y., Lv, H., Xing, H., Zhao, T., Yu, D., & Chen, S. (2007). Identification, inheritance and QTL mapping of root traits related to tolerance to rhizo-spheric stresses in soybean (*G. max* (L.) Merr.). *Frontiers of Agriculture in China*, *1*, 119-128.
Garbout, A., Munkholm, L. J., Hansen, S. B., Petersen, B. M., Munk, O. L., & Pajor, R. (2012). The use of PET/CT scanning technique for 3D visualization and quantification of real-time soil/plant interactions. *Plant and soil*, *352*(1-2), 113-127. https://doi.org/10.1007/s11104-011-0983-8

Geigenberger, P., Tiessen, A., & Meurer, J. (2011). Use of non-aqueous fractionation and metabolomics to study chloroplast function in Arabidopsis. *Chloroplast Research in Arabidopsis: Methods and Protocols, Volume II*, 135-160.
Giehl, R. F., Gruber, B. D., & von Wirén, N. (2014). It's time to make changes: modulation of root system architecture by nutrient signals. *Journal of Experimental Botany*, *65*(3), 769-778.
Giuliani, S., Sanguineti, M. C., Tuberosa, R., Bellotti, M., Salvi, S., & Landi, P. (2005). Root-ABA1, a major constitutive QTL, affects maize root architecture and leaf ABA concentration at different water regimes. *Journal of Experimental Botany*, *56*(422), 3061-3070.
Goss, M. (1977). Effects of mechanical impedance on root growth in barley (*Hordeum vulgare* L.) I. Effects on the elongation and branching of seminal root axes. *Journal of Experimental Botany*, *28*(1), 96-111.
Gregory, P. J., Hutchison, D., Read, D. B., Jenneson, P. M., Gilboy, W. B., & Morton, E. J. (2003). Non-invasive imaging of roots with high resolution X-ray micro-tomography. Roots: The Dynamic Interface between Plants and the Earth: The 6th Symposium of the International Society of Root Research, 11–15 November 2001, Nagoya, Japan,
Grift, T., Novais, J., & Bohn, M. (2011). High-throughput phenotyping technology for maize roots. *Biosystems engineering*, *110*(1), 40-48.
Grzesiak, S., Grzesiak, M. T., Filek, W., Hura, T., & Stabryła, J. (2002). The impact of different soil moisture and soil compaction on the growth of triticale root system. *Acta Physiologiae Plantarum*, *24*, 331-342.
Gul, M. U., Paul, A., & Chehri, A. (2023). Hydrotropism: understanding the impact of water on plant movement and adaptation. *Water*, *15*(3), 567.
Han, L., Dutilleul, P., Prasher, S. O., Beaulieu, C., & Smith, D. L. (2008). Assessment of Common Scab-Inducing Pathogen Effects on Potato Underground Organs Via Computed Tomography Scanning. *Phytopathology*, *98*(10), 1118.
Han, L., Dutilleul, P., Prasher, S. O., Beaulieu, C., & Smith, D. L. (2009). Assessment of Density Effects of the Common Scab-Inducing Pathogen on the Seed and Peripheral Organs of Potato During Growth Using Computed Tomography Scanning Data. *Transactions of the ASABE*, *52*(1), 305-311. https://doi.org/10.13031/2013.25924
Hargreaves, C. E., Gregory, P. J., & Bengough, A. G. (2009). Measuring root traits in barley (Hordeum vulgare ssp. vulgare and ssp. spontaneum) seedlings using gel chambers, soil sacs and X-ray microtomography. *Plant and soil*, *316*, 285-297.
Hauck, A. L., Novais, J., Grift, T. E., & Bohn, M. O. (2015). Characterization of mature maize (*Zea mays* L.) root system architecture and complexity in a diverse set of Ex-PVP inbreds and hybrids. *SpringerPlus*, *4*(1), 424. https://doi.org/10.1186/s40064-015-1187-0
Hirai, M. Y., Yano, M., Goodenowe, D. B., Kanaya, S., Kimura, T., Awazuhara, M., Arita, M., Fujiwara, T., & Saito, K. (2004). Integration of transcriptomics and metabolomics for understanding of global responses to nutritional stresses in Arabidopsis thaliana. *Proceedings of the National Academy of Sciences*, *101*(27), 10205-10210.
Hodge, A., Berta, G., Doussan, C., Merchan, F., & Crespi, M. (2009). Plant root growth, architecture and function. In: Springer.
Huang, B., & Fry, J. D. (1998). Root anatomical, physiological, and morphological responses to drought stress for tall fescue cultivars. *Crop Science*, *38*(4), 1017-1022.
Huang, L., Zhang, Y., Guo, J., Peng, Q., Zhou, Z., Duan, X., Tanveer, M., & Guo, Y. (2023). High-throughput root phenotyping of crop cultivars tolerant to low N in waterlogged soils. *Frontiers in Plant Science*, *14*, 1271539.

Hund, A., Trachsel, S., & Stamp, P. (2009). Growth of axile and lateral roots of maize: I development of a phenotying platform. *Plant and soil*, *325*, 335-349.
Islam, I., Adam, Z., & Islam, S. (2019). Soybean (Glycine Max): alternative sources of human nutrition and bioenergy for the 21st century. *Am. J. Food Sci. Technol*, *7*, 1-6.
Jahnke, S., Menzel, M. I., Van Dusschoten, D., Roeb, G. W., Bühler, J., Minwuyelet, S., Blümler, P., Temperton, V. M., Hombach, T., Streun, M., Beer, S., Khodaverdi, M., Ziemons, K., Coenen, H. H., & Schurr, U. (2009). Combined MRI–PET dissects dynamic changes in plant structures and functions. *The Plant Journal*, *59*(4), 634-644. https://doi.org/10.1111/j.1365-313x.2009.03888.x
Jenneson, P., Gilboy, W., Morton, E., Luggar, R., Gragory, P., & Hutchinson, D. (1999). Optimisation of X-ray micro-tomography for the in situ study of the development of plant roots. 1999 IEEE Nuclear Science Symposium. Conference Record. 1999 Nuclear Science Symposium and Medical Imaging Conference (Cat. No. 99CH37019),
Kadam, N. N., Tamilselvan, A., Lawas, L. M., Quinones, C., Bahuguna, R. N., Thomson, M. J., Dingkuhn, M., Muthurajan, R., Struik, P. C., & Yin, X. (2017). Genetic control of plasticity in root morphology and anatomy of rice in response to water deficit. *Plant physiology*, *174*(4), 2302-2315.
Kalender, W. A. (2011). *Computed tomography: fundamentals, system technology, image quality, applications*. John Wiley & Sons.
Kanase, T., Guhey, A., & Gawas, D. (2019). Activity of antioxidant enzymes in soybean genotypes under drought stress. *International Journal of Current Microbiology and Applied Sciences*, *8*, 2323-2330.
Kuijken, R. C., van Eeuwijk, F. A., Marcelis, L. F., & Bouwmeester, H. J. (2015). Root phenotyping: from component trait in the lab to breeding. *Journal of Experimental Botany*, *66*(18), 5389-5401.
Lafond, J. A., Han, L., & Dutilleul, P. (2015). Concepts and analyses in the CT scanning of root systems and leaf canopies: A timely summary. *Frontiers in Plant Science*, *6*, 165179.
Lakhiar, I. A., Jianmin, G., Syed, T. N., Chandio, F. A., Buttar, N. A., & Qureshi, W. A. (2018). Monitoring and control systems in agriculture using intelligent sensor techniques: A review of the aeroponic system. *Journal of Sensors*, *2018*, 1-18.
Landi, P., Sanguineti, M. C., Liu, C., Li, Y., Wang, T., Giuliani, S., Bellotti, M., Salvi, S., & Tuberosa, R. (2007). Root-ABA1 QTL affects root lodging, grain yield, and other agronomic traits in maize grown under well-watered and water-stressed conditions. *Journal of Experimental Botany*, *58*(2), 319-326.
Le Marié, C., Kirchgessner, N., Marschall, D., Walter, A., & Hund, A. (2014). Rhizoslides: paper-based growth system for non-destructive, high throughput phenotyping of root development by means of image analysis. *Plant Methods*, *10*, 1-16.
Lei, X., Shen, Y., Zhao, J., Huang, J., Wang, H., Yu, Y., & Xiao, C. (2023). Root exudates mediate the processes of soil organic carbon input and efflux. *Plants*, *12*(3), 630.
Lisec, J., Schauer, N., Kopka, J., Willmitzer, L., & Fernie, A. R. (2006). Gas chromatography mass spectrometry–based metabolite profiling in plants. *Nature protocols*, *1*(1), 387-396.
Lontoc-Roy, M., Dutilleul, P., Prasher, S. O., Han, L., Brouillet, T., & Smith, D. L. (2006). Advances in the acquisition and analysis of CT scan data to isolate a crop root system from the soil medium and quantify root system complexity in 3-D space. *Geoderma*, *137*(1-2), 231-241.

Lontoc-Roy, M., Dutilleul, P., Prasher, S. O., Han, L., & Smith, D. L. (2005). Computed tomography scanning for three-dimensional imaging and complexity analysis of developing root systems. *Botany*, *83*(11), 1434-1442.
Lynch, J. (1995). Root architecture and plant productivity. *Plant physiology*, *109*(1), 7.
Lynch, J. P. (2022). Harnessing root architecture to address global challenges. *The Plant Journal*, *109*(2), 415-431.
Malamy, J. (2005). Intrinsic and environmental response pathways that regulate root system architecture. *Plant, cell & environment*, *28*(1), 67-77.
Mandelbrot, B. B. (1982). *The fractal geometry of nature* (Vol. 1). WH freeman New York.
Mao, B., Takahashi, H., Takahashi, H., & Fujii, N. (2022). Diversity of root hydrotropism among natural variants of Arabidopsis thaliana. *Journal of Plant Research*, *135*(6), 799-808.
Masclaux-Daubresse, C., Clément, G., Anne, P., Routaboul, J.-M., Guiboileau, A., Soulay, F., Shirasu, K., & Yoshimoto, K. (2014). Stitching together the multiple dimensions of autophagy using metabolomics and transcriptomics reveals impacts on metabolism, development, and plant responses to the environment in Arabidopsis. *The Plant Cell*, *26*(5), 1857-1877.
Mochida, K., & Shinozaki, K. (2010). Genomics and bioinformatics resources for crop improvement. *Plant and Cell Physiology*, *51*(4), 497-523.
Mooney, S. J., Pridmore, T. P., Helliwell, J., & Bennett, M. J. (2012). Developing X-ray Computed Tomography to non-invasively image 3-D root systems architecture in soil. *Plant and soil*, *352*(1-2), 1-22. https://doi.org/10.1007/s11104-011-1039-9
Morris, E. C., Griffiths, M., Golebiowska, A., Mairhofer, S., Burr-Hersey, J., Goh, T., Von Wangenheim, D., Atkinson, B., Sturrock, C. J., & Lynch, J. P. (2017). Shaping 3D root system architecture. *Current biology*, *27*(17), R919-R930.
Morrison, M., McLaughlin, N., Cober, E., & Butler, G. (2006). When is short-season soybean most susceptible to water stress? *Canadian journal of plant science*, *86*(Special Issue), 1327-1331.
Nagel, K. A., Kastenholz, B., Jahnke, S., Van Dusschoten, D., Aach, T., Mühlich, M., Truhn, D., Scharr, H., Terjung, S., & Walter, A. (2009). Temperature responses of roots: impact on growth, root system architecture and implications for phenotyping. *Functional Plant Biology*, *36*(11), 947-959.
Nagel, K. A., Putz, A., Gilmer, F., Heinz, K., Fischbach, A., Pfeifer, J., Faget, M., Blossfeld, S., Ernst, M., & Dimaki, C. (2012). GROWSCREEN-Rhizo is a novel phenotyping robot enabling simultaneous measurements of root and shoot growth for plants grown in soil-filled rhizotrons. *Functional Plant Biology*, *39*(11), 891-904.
Osmont, K. S., Sibout, R., & Hardtke, C. S. (2007). Hidden branches: developments in root system architecture. *Annu. Rev. Plant Biol.*, *58*, 93-113.
Osvald, J., Petrovic, N., & Demsar, J. (2001). Sugar and organic acid content of tomato fruits (Lycopersicon lycopersicum Mill.) grown on aeroponics at different plant density. *Acta Alimentaria*, *30*(1), 53-61.
Palmer, C. M., Bush, S. M., & Maloof, J. N. (2012). Phenotypic and Developmental Plasticity in Plants. *eLS*. https://doi.org/10.1002/9780470015902.a0002092.pub2
Palmer, L. J., Dias, D. A., Boughton, B., Roessner, U., Graham, R. D., & Stangoulis, J. R. (2014). Metabolite profiling of wheat (Triticum aestivum L.) phloem exudate. *Plant Methods*, *10*, 1-9.
Pfeifer, J., Faget, M., Walter, A., Blossfeld, S., Fiorani, F., Schurr, U., & Nagel, K. A. (2014). Spring barley shows dynamic compensatory root and shoot growth responses when exposed to localised soil compaction and fertilisation. *Functional Plant Biology*, *41*(6), 581-597.

Piekarska-Stachowiak, A., & Nakielski, J. (2013). The simulation model of growth and cell divisions for the root apex with an apical cell in application to Azolla pinnata. *Planta*, *238*, 1051-1064.
Popova, L., van Dusschoten, D., Nagel, K. A., Fiorani, F., & Mazzolai, B. (2016). Plant root tortuosity: an indicator of root path formation in soil with different composition and density. *Annals of Botany*, *118*(4), 685-698.
Rellán-Álvarez, R., Lobet, G., Lindner, H., Pradier, P.-L., Sebastian, J., Yee, M.-C., Geng, Y., Trontin, C., LaRue, T., & Schrager-Lavelle, A. (2015). GLO-Roots: an imaging platform enabling multidimensional characterization of soil-grown root systems. *elife*, *4*, e07597.
Rich, S. M., & Watt, M. (2013). Soil conditions and cereal root system architecture: review and considerations for linking Darwin and Weaver. *Journal of Experimental Botany*, *64*(5), 1193-1208.
Rogers, E. D., Monaenkova, D., Mijar, M., Nori, A., Goldman, D. I., & Benfey, P. N. (2016). X-Ray Computed Tomography Reveals the Response of Root System Architecture to Soil Texture *Plant physiology*, *171*(3), 2028-2040. https://doi.org/10.1104/pp.16.00397
Ruiz, S., Or, D., & Schymanski, S. J. (2015). Soil Penetration by Earthworms and Plant Roots—Mechanical Energetics of Bioturbation of Compacted Soils. *PloS one*, *10*(6), e0128914. https://doi.org/10.1371/journal.pone.0128914
Sánchez-Calderón, L., López-Bucio, J., Chacón-López, A., Gutiérrez-Ortega, A., Hernández-Abreu, E., & Herrera-Estrella, L. (2006). Characterization of low phosphorus insensitive mutants reveals a crosstalk between low phosphorus-induced determinate root development and the activation of genes involved in the adaptation of Arabidopsis to phosphorus deficiency. *Plant physiology*, *140*(3), 879-889.
Sanghera, P., Belzile, F., Seck, W., & Dutilleul, P. (2023). Cluster Analysis of 137 Soybean Lines Based on Root System Architecture Traits Measured in Rhizoboxes.
Seck, W., Torkamaneh, D., & Belzile, F. (2020). Comprehensive genome-wide association analysis reveals the genetic basis of root system architecture in soybean. *Frontiers in Plant Science*, *11*, 590740.
Selvaraj, M. G., Montoya-P, M. E., Atanbori, J., French, A. P., & Pridmore, T. (2019). A low-cost aeroponic phenotyping system for storage root development: unravelling the below-ground secrets of cassava (*Manihot esculenta*). *Plant Methods*, *15*, 1-13.
Singh, I., Pathak, J., Mahajan, M., Nehte, D., & Singh, L. (2018). Enhancing soybean yield through improved production technology under frontline demonstration in Madhya Pradesh and Maharashtra. *Journal of Community Mobilization and Sustainable Development*, *13*(3), 442-446.
Slovak, R., Göschl, C., Su, X., Shimotani, K., Shiina, T., & Busch, W. (2014). A scalable open-source pipeline for large-scale root phenotyping of Arabidopsis. *The Plant Cell*, *26*(6), 2390-2403.
Sriyudthsak, K., Iwata, M., Hirai, M. Y., & Shiraishi, F. (2014). PENDISC: a simple method for constructing a mathematical model from time-series data of metabolite concentrations. *Bulletin of mathematical biology*, *76*, 1333-1351.
Subramanian, S., Han, L., Dutilleul, P., & Smith, D. L. (2015). Computed tomography scanning can monitor the effects of soil medium on root system development: an example of salt stress in corn. *Frontiers in Plant Science*, *6*. https://doi.org/10.3389/fpls.2015.00256
Sultan, S. E., & Spencer, H. G. (2002). Metapopulation structure favors plasticity over local adaptation. *The American Naturalist*, *160*(2), 271-283.

Tatsumi, J., Yamauchi, A., & Kono, Y. (1989). Fractal analysis of plant root systems. *Annals of Botany*, *64*(5), 499-503.
Tohge, T., de Souza, L. P., & Fernie, A. R. (2014). Genome-enabled plant metabolomics. *Journal of Chromatography B*, *966*, 7-20.
Tollner, E. (1991). X-ray computed tomography applications in soil ecology studies. *Agriculture, Ecosystems & Environment*, *34*(1-4), 251-260.
Tollner, E., Ramseur, E., & Murphy, C. (1994). Techniques and approaches for documenting plant root development with x-ray computed tomography. *Tomography of Soil-Water-Root Processes*, *36*, 115-133.
Topp, C. N., Iyer-Pascuzzi, A. S., Anderson, J. T., Lee, C.-R., Zurek, P. R., Symonova, O., Zheng, Y., Bucksch, A., Mileyko, Y., Galkovskyi, T., Moore, B. T., Harer, J., Edelsbrunner, H., Mitchell-Olds, T., Weitz, J. S., & Benfey, P. N. (2013). 3D phenotyping and quantitative trait locus mapping identify core regions of the rice genome controlling root architecture. *Proceedings of the National Academy of Sciences*, *110*(18), E1695-E1704. https://doi.org/10.1073/pnas.1304354110
Trachsel, S., Kaeppler, S. M., Brown, K. M., & Lynch, J. P. (2011). Shovelomics: high throughput phenotyping of maize (*Zea mays* L.) root architecture in the field. *Plant and soil*, *341*, 75-87.
Usadel, B., Schwacke, R., Nagel, A., & Kersten, B. (2012). GabiPD–the GABI Primary Database integrates plant proteomic data with gene-centric information. *Frontiers in Plant Science*, *3*, 154.
Verslues, P. E., Agarwal, M., Katiyar-Agarwal, S., Zhu, J., & Zhu, J. K. (2006). Methods and concepts in quantifying resistance to drought, salt and freezing, abiotic stresses that affect plant water status. *The Plant Journal*, *45*(4), 523-539.
Via, S., Gomulkiewicz, R., De Jong, G., Scheiner, S. M., Schlichting, C. D., & Van Tienderen, P. H. (1995). Adaptive phenotypic plasticity: consensus and controversy. *Trends in ecology & evolution*, *10*(5), 212-217.
Waidmann, S., Sarkel, E., & Kleine-Vehn, J. (2020). Same same, but different: growth responses of primary and lateral roots. *Journal of Experimental Botany*, *71*(8), 2397-2411.
Walk, T. C., Van Erp, E., & Lynch, J. P. (2004). Modelling applicability of fractal analysis to efficiency of soil exploration by roots. *Annals of Botany*, *94*(1), 119-128.
Wang, H., Siopongco, J., Wade, L. J., & Yamauchi, A. (2009). Fractal analysis on root systems of rice plants in response to drought stress. *Environmental and Experimental Botany*, *65*(2-3), 338-344.
Wang, Y., Zhou, E., Yao, M., Xue, D., Zhao, N., Zhou, Y., Li, B., Wang, K., Miao, Y., Gu, C., Wang, X., & Wei, L. (2023). PEG-6000 Priming Improves Aged Soybean Seed Vigor via Carbon Metabolism, ROS Scavenging, Hormone Signaling, and Lignin Synthesis Regulation. *Agronomy*, *13*(12), 3021. https://www.mdpi.com/2073-4395/13/12/3021
Watanabe, Y., Kabuki, T., Kakehashi, T., Kano-Nakata, M., Mitsuya, S., & Yamauchi, A. (2020). Morphological and histological differences among three types of component roots and their differential contribution to water uptake in the rice root system. *Plant Production Science*, *23*(2), 191-201.
Weihs, B. J., Heuschele, D.-J., Tang, Z., York, L. M., Zhang, Z., & Xu, Z. (2024). The State of the Art in Root System Architecture Image Analysis Using Artificial Intelligence: A Review. *Plant Phenomics*, *6*, 0178. https://doi.org/doi:10.34133/plantphenomics.0178

Wildenschild, D., Vaz, C., Rivers, M., Rikard, D., & Christensen, B. (2002). Using X-ray computed tomography in hydrology: systems, resolutions, and limitations. *Journal of Hydrology*, *267*(3-4), 285-297.

Wojciechowski, T., Gooding, M., Ramsay, L., & Gregory, P. (2009). The effects of dwarfing genes on seedling root growth of wheat. *Journal of Experimental Botany*, *60*(9), 2565-2573.

Xiong, R., Liu, S., Considine, M. J., Siddique, K. H. M., Lam, H. M., & Chen, Y. (2021). Root system architecture, physiological and transcriptional traits of soybean (*Glycine max* L.) in response to water deficit: A review. *Physiologia Plantarum*, *172*(2), 405-418. https://doi.org/10.1111/ppl.13201

Ytting, N., Andersen, S., & Thorup-Kristensen, K. (2014). Using tube rhizotrons to measure variation in depth penetration rate among modern North-European winter wheat (*Triticum aestivum* L.) cultivars. *Euphytica*, *199*, 233-245.

Yu, Y.-J., Xia, Q.-L., Wang, S., Wang, B., Xie, F.-W., Zhang, X.-B., Ma, Y.-M., & Wu, H.-L. (2014). Chemometric strategy for automatic chromatographic peak detection and background drift correction in chromatographic data. *Journal of Chromatography A*, *1359*, 262-270.

Zappala, S., Helliwell, J. R., Tracy, S. R., Mairhofer, S., Sturrock, C. J., Pridmore, T., Bennett, M., & Mooney, S. J. (2013). Effects of X-ray dose on rhizosphere studies using X-ray computed tomography. *PloS one*, *8*(6), e67250.

Zhang, W., Shen, X., Wu, P., Hu, B., & Liao, C. (2001). QTLs and epistasis for seminal root length under a different water supply in rice (*Oryza sativa* L.). *Theoretical and Applied Genetics*, *103*, 118-123.

Zhu, J., Mickelson, S. M., Kaeppler, S. M., & Lynch, J. P. (2006). Detection of quantitative trait loci for seminal root traits in maize (*Zea mays* L.) seedlings grown under differential phosphorus levels. *Theoretical and Applied Genetics*, *113*, 1-10.

Appendices

Appendix A: SAS Scripts

A1. Cluster analysis with the 12 RSA-related traits (Approach 1)

```
PROC FASTCLUS DATA=work.soybean_scores MAXC=30 OUT=work.fastclus_scores;
VAR TLR LPR LSR DTLR TNR MED MAX DRS WRS RS DR SAR;
RUN;
PROC PRINT DATA=work.fastclus_scores;
RUN;
```

A2. Principal component analysis (PCA) on the estimated correlation matrix of the 12 RSA-related variables

(Approach 2)

```
PROC PRINCOMP DATA=PCA_Seck_et_al_2020 STANDARD OUT=work.soybean_scores
PLOTS=ALL;
VAR TLR LPR LSR DTLR TNR Med Max DRS WRS RS DR SAR;
RUN;
PROC PRINT DATA=work.soybean_scores;
RUN;
```

A3. Cluster analysis with the first 6 principal components accounting for 95% variability in the PCA

(Approach 2)

```
PROC FASTCLUS DATA=work.soybean_scores MAXC=30 OUT=work.fastclus_scores;
VAR Prin1-Prin6;
RUN;
PROC PRINT DATA=work.fastclus_scores;
RUN;
```

Appendix B: Supplementary Tables

Table B 1: Numerical information presented in supplement to that in Table 3.1 (left half)

Cluster analysis performed on the dataset for the 12 RSA-related traits, including the distance to the centroid and the 12 mean values for each of the 137 soybean lines. White and yellow colours are used to highlight lines that are members of different clusters from Cluster 1 to Cluster 30, while red is used to identify clusters with only one member.

Distance	Cluster	Line	TLR	LPR	LSR	DTLR	TNR	Med	Max	DRS	WRS	RS	DR	SAR
1.232596	1	4004P4J	-0.3485	0.0848	-0.2872	-0.2995	-2.5140	0.2320	-1.0961	-0.1580	1.2019	1.1909	0.5750	-0.1815
1.232596	1	5017_25B	-0.4256	0.1719	-0.3576	-0.6252	-1.5277	-1.5012	-1.3444	-0.6144	0.3641	0.3062	0.8588	-0.5563
0	2	4005_24j	0.2243	0.1719	0.1985	0.6775	-2.1757	-0.6182	-1.5354	0.8200	1.5242	1.7296	-2.0926	0.8152
0.969116	3	PS44	0.0233	2.1743	-0.0557	0.3518	0.7545	-0.9453	-1.3444	0.5592	1.0730	1.1512	-0.2196	0.6234
1.323891	3	SECAN9-3	0.3382	1.3908	0.2825	0.6775	1.4961	-1.1742	-1.2871	0.8852	0.3641	0.3062	-0.7872	0.8501
1.421002	3	Phoenix	0.5426	2.6967	0.4550	1.0032	0.8985	-0.7491	-1.2107	1.1460	1.3308	1.3100	-0.9574	1.1029
1.496352	3	OAC9-48C	-0.1609	1.8696	-0.2362	0.0262	0.2938	-1.5993	-0.0648	0.2984	0.7508	0.7485	-0.9007	0.4752
1.497452	3	Hercule	0.3751	0.9119	0.3313	0.6775	-0.3542	-0.5201	-0.9624	0.9504	0.8797	0.9640	-1.1845	0.9227
1.385713	4	Jari	-0.2960	2.1308	-0.3315	0.0262	-0.3254	0.4609	1.3866	0.1028	0.7508	0.8052	1.1426	0.0888
1.566451	4	SECAN7-2	-0.2369	1.3037	-0.2498	0.0262	1.2297	0.5591	-0.0075	0.1680	1.0086	1.1115	2.1643	0.3648

1.696042	4	SECAN8-1	-0.3027	1.3037	-0.2736	0.0262	1.4457	0.7880	1.1384	0.0376	0.1063	0.0623	0.4048	0.0859
1.852344	4	OACAyton	-0.3117	1.2602	-0.2816	-0.2995	0.2938	2.1942	1.5585	-0.0276	0.9441	1.0888	2.1643	-0.0391
2.020686	4	Misty	-0.2592	0.9555	-0.2645	0.0262	0.0778	0.6899	-0.0648	0.1680	1.5242	1.7296	-0.2196	0.1701
0	5	Tundra	-0.0593	-0.3069	-0.0750	0.3518	1.8057	-0.4220	-1.3444	0.4288	3.1998	2.3875	-0.4466	0.5363
0	6	Delta	-0.2614	-1.4823	-0.2033	0.0262	-0.5414	2.8155	1.7113	0.1028	1.3308	1.3383	1.7102	0.1672
1.222566	7	OAC7-26C	3.9909	1.1731	3.9801	3.2831	0.1066	-1.5993	-0.5232	2.3196	0.6219	0.6918	-0.6736	1.9456
1.222566	7	OACBayfield	4.6777	-0.3505	4.7178	3.2831	0.3226	-0.5201	-0.5805	2.3848	-0.0870	-0.0738	-0.1628	2.2159
1.379225	8	Casino	-0.9058	0.3460	-0.9466	-1.9280	-0.6638	0.6899	1.0047	-1.4620	-0.6671	-2.4954	-0.9574	-3.0612
1.379225	8	Colby	-0.7695	-1.3952	-0.7628	-1.2766	-0.6134	0.4609	0.4317	-1.6576	-1.3760	-1.3498	-1.2980	-1.7390
1.880963	8	Altona	-0.7092	-1.7870	-0.7060	-1.2766	-0.7862	-0.1931	0.5081	-1.5924	-1.4404	-1.4462	-0.7304	-1.6373
0	9	5055_43G	-0.4044	-0.4375	-0.3644	-0.2995	-1.3837	1.5401	0.3744	-0.4188	-1.9560	-1.6334	-2.3764	-0.3035
1.251672	10	Costaud	0.2076	-0.6552	0.2031	0.6775	-0.5918	-0.4220	-0.1412	0.8200	0.2352	0.1360	-0.6169	0.7920
1.381823	10	5070_26j	0.3907	-2.4399	0.4346	1.0032	-1.3621	0.1339	-0.8287	1.0156	-0.3448	-0.2156	-0.4466	0.9344
1.80892	10	KG-41	0.0378	-1.1776	0.0430	0.3518	-0.3038	0.8861	0.1262	0.5592	-0.8604	-0.6523	-1.4115	0.6380
1.839598	10	DH618	-0.0627	-0.4375	-0.0750	0.3518	-0.5702	-0.6182	0.4699	0.3636	-0.6026	-0.6126	-1.2412	0.5305
1.87685	10	5146_41j	0.4075	-1.0034	0.4141	1.0032	-1.1893	-1.1742	-1.0197	1.0156	-0.9893	-0.9018	0.6886	1.0506
1.357312	11	Madoc	-0.7316	-0.6987	-0.7571	-1.2766	-0.1598	0.3628	0.5654	-1.6576	-1.2471	-1.2080	0.4048	-1.6635

1.497941	11	OAC1-26	-0.5573	-0.8728	-0.5642	-0.6252	0.1066	-0.0950	1.4630	-0.9404	-1.1182	-0.9642	0.6318	-0.8062
1.721228	11	Victoria	-0.6791	-1.3081	-0.6879	-0.9509	1.9064	-0.4220	0.0498	-1.3968	-1.9560	-1.6447	0.4615	-1.5095
1.766948	11	OT09-03	-0.5216	-1.3517	-0.5244	-0.6252	0.5097	-1.1742	-0.5805	-0.7448	-1.4404	-1.4633	-0.8439	-0.7394
1.10394	12	MapleAmbr	-0.0761	-0.2199	-0.0943	0.3518	-0.1382	-0.2912	-0.0648	0.3636	0.3641	0.2381	-0.2196	0.4956
1.282034	12	OAC9-22C	-0.2581	-0.0893	-0.2362	0.0262	0.2506	-1.2723	-1.0961	0.1680	0.5575	0.5273	-0.3899	0.1788
1.326013	12	Naya	0.0825	0.0413	0.0578	0.6775	0.0778	-1.7301	-0.1412	0.7548	0.6863	0.7202	0.9724	0.6641
1.397447	12	OT05-20	-0.3039	-0.0022	-0.2396	0.0262	0.5097	-0.5201	-0.3322	0.0376	-0.0870	-0.1248	0.5183	-0.0217
1.400147	12	MapleRidge	-0.2257	0.3460	-0.2135	0.0262	0.0346	-0.4220	-1.2871	0.2332	0.0419	-0.0114	-0.0493	0.3735
1.426872	12	Katrina	0.1238	-0.0458	0.1020	0.6775	-0.1814	0.2320	0.1835	0.7548	0.8152	0.8052	0.6318	0.7397
1.510466	12	OACChampion	-0.2927	0.1284	-0.2770	0.0262	0.3442	-0.2912	-0.0648	0.1028	1.3953	1.4744	0.4615	0.1120
1.567332	12	KORADA	-0.2536	0.6507	-0.2498	0.0262	-0.2534	-0.7491	-0.5805	0.1680	1.2664	1.2533	1.3697	0.2515
1.664315	12	Bloomfield	-0.3117	-0.8728	-0.2248	0.0262	-0.7574	-0.4220	-0.0648	0.0376	0.4930	0.5217	-0.2196	-0.0362
1.745247	12	OT11-03	0.3516	-1.1776	0.3619	0.6775	0.6105	-0.5201	-0.5805	0.8852	1.0086	1.1398	0.8021	0.8763
2.011681	12	Bravor	0.2556	-0.0022	0.2348	0.6775	-0.7358	-1.8283	-1.7264	0.8200	0.2997	0.2041	0.5183	0.8298
0.898254	13	OAC8-21C	3.2617	-0.3505	3.2775	2.3060	0.1786	-1.1742	-0.4468	1.8632	1.9753	1.9792	-0.2763	1.7654
1.574772	13	OT94-47	3.8792	-1.0470	3.9245	2.9574	0.6321	-0.9453	-0.1985	2.2544	2.1042	2.1209	-0.2196	1.8148
2.085458	13	MapleArrow	2.4867	-0.8293	2.5035	2.3060	-0.1382	-1.0761	-1.2871	1.8632	0.3641	0.3118	0.1777	1.6957

0	14	Woodstock	4.7804	-0.8293	4.8335	3.9344	4.5703	0.2320	2.2842	3.0367	2.2331	2.2797	0.2345	2.3641
1.191081	15	S05-T6	0.0077	0.4766	-0.0273	0.3518	1.1577	0.0358	0.1835	0.4288	0.2997	0.2268	0.4048	0.5392
1.23831	15	SECAN7-4	0.0122	-1.3952	0.0260	0.3518	1.2297	0.5591	0.8137	0.4288	0.5575	0.6011	1.0291	0.5508
1.333946	15	Supra	0.2277	-1.0034	0.2314	0.6775	1.7625	1.2131	1.0811	0.8200	0.1063	0.0566	0.6318	0.8181
1.443426	15	Ohgata	-0.2424	0.6507	-0.2384	0.0262	0.6321	0.5591	1.3293	0.1680	0.4286	0.4139	0.0642	0.3154
1.447583	16	Albinos	-0.8108	-2.5705	-0.7741	-1.2766	-0.8078	-0.4220	-0.7142	-1.7228	-0.2159	-0.1816	0.1210	-1.7448
1.508762	16	ACGlengarry	-0.7394	-1.4387	-0.7310	-1.2766	-0.9518	-1.4031	-1.0961	-1.6576	-1.7627	-1.5653	0.6318	-1.7390
1.67886	16	9004	-0.8778	-1.0034	-0.8831	-1.9280	-1.1893	-0.7491	-0.6951	-1.2012	-0.8604	-2.2969	0.4615	-1.9599
1.780846	16	Dundas	-0.8644	-2.1788	-0.8388	-1.6023	-0.4982	-0.5201	-0.0648	-1.7228	0.0419	0.0056	1.6535	-1.9366
2.567814	16	4028P7j	-0.6143	-0.5681	-0.6300	-0.9509	-1.8877	-0.7491	-0.0075	-1.1360	-1.9560	-1.8092	1.1426	-1.0503
1.088592	17	OAC9-35C	-0.6701	0.4766	-0.7253	-0.9509	0.2722	1.3439	1.4630	-1.2664	-0.4737	-0.5388	0.3480	-1.2741
1.446458	17	OAC7-3C	-0.5272	-0.7858	-0.5449	-0.6252	0.1066	2.7501	2.3415	-0.8100	-0.8604	-0.7544	0.3480	-0.7743
1.800249	17	SECAN8-1	-0.6746	-1.1776	-0.6867	-0.9509	1.3737	1.4420	1.5776	-1.3316	-1.4404	-1.3612	0.2345	-1.3787
1.854362	17	Amasa	-0.6936	-0.0458	-0.7355	-1.2766	-0.7574	1.1150	1.0811	-1.4620	-1.4404	-1.3555	1.3697	-1.5327
2.037467	17	90A07	-0.4758	-0.6552	-0.3871	-0.6252	-1.0237	2.3250	1.8450	-0.6796	-1.4404	-1.4633	-0.6736	-0.6319
2.047961	17	PS36	-0.5339	0.4766	-0.5834	-0.6252	0.6825	1.3439	1.2720	-0.8100	0.2997	0.1814	0.9724	-0.7772
1.169068	18	Clinton	-0.4457	-0.7858	-0.3531	-0.6252	-0.6638	-0.2912	-0.5232	-0.6144	-1.1826	-0.9869	0.0642	-0.5796

1.174657	18	OT11-01	-0.5406	-0.9599	-0.5528	-0.6252	0.5385	-0.8472	-1.2871	-0.8100	-0.4093	-0.4424	-0.2196	-0.7859
1.209177	18	Alta	-0.6132	-0.5246	-0.6288	-0.9509	-0.7862	-0.6182	-0.5232	-1.0708	-0.9249	-0.7884	0.8021	-1.0358
1.275985	18	OAC9-17C	-0.5864	-0.7422	-0.5982	-0.9509	0.1786	-0.1931	-1.1534	-1.0056	-0.2159	-0.1872	0.8021	-0.8585
1.443737	18	DH530	-0.5886	0.1719	-0.6232	-0.9509	-0.5702	-0.5201	-0.6378	-1.0708	-1.2471	-1.1457	0.7453	-0.9021
1.487421	18	Madison	-0.6433	-0.0458	-0.6833	-0.9509	-0.1598	-1.4031	-1.2107	-1.1360	-0.2159	-0.2042	0.9724	-1.1578
1.58304	18	OAC8-22C	-0.3385	-1.3952	-0.2396	-0.2995	0.1786	-1.5012	-1.2871	-0.0928	-0.8604	-0.7090	1.2562	-0.0565
1.653653	18	Purdy	-0.3865	-0.7422	-0.3383	-0.2995	1.0857	-0.0950	-1.2107	-0.3536	-0.9249	-0.8281	0.0642	-0.2628
1.945617	18	90B11	-0.3385	-0.9599	-0.2498	-0.2995	-0.9734	-1.7301	-2.2420	-0.0928	-0.5382	-0.5559	0.0642	-0.0478
1.057824	19	MapleIsle	-0.4769	0.2154	-0.4109	-0.6252	-0.0374	0.3628	-0.3322	-0.6796	-1.2471	-1.0890	-0.0493	-0.6464
1.263809	19	AC2001	-0.4044	-0.2199	-0.3701	-0.2995	-0.9518	0.7880	-0.3895	-0.3536	-0.9249	-0.8961	0.3480	-0.2803
1.429133	19	Lotus	-0.1978	-0.2199	-0.1703	0.0262	-0.1814	0.8861	0.3744	0.2332	-0.5382	-0.5956	-0.3331	0.4084
1.467523	19	Heather	-0.4088	0.6507	-0.3973	-0.6252	-0.3758	1.1150	0.8901	-0.4840	-0.6026	-0.6182	-0.7872	-0.3558
1.487397	19	Gretna	-0.6165	0.3460	-0.6549	-0.9509	-0.3974	0.6899	0.3744	-1.1360	-0.5382	-0.5729	-0.0493	-1.0561
1.525628	19	OT11-02	-0.4602	1.4343	-0.4257	-0.6252	0.5817	0.2320	0.2407	-0.6144	-0.8604	-0.7544	0.4615	-0.5999
1.614869	19	OAC9-44C	-0.3429	0.3460	-0.2884	-0.2995	0.2722	2.0961	-0.9624	-0.1580	-0.7960	-0.6466	0.5183	-0.0798
1.659508	19	OAC8-11C	-0.4211	1.2602	-0.3814	-0.6252	0.1498	0.6899	-0.1030	-0.5492	0.1708	0.0793	-0.7872	-0.4314
2.352987	19	Perth	-0.1944	0.3460	-0.1817	0.0262	0.7545	0.2320	1.2720	0.2984	-1.1826	-1.0096	-0.9007	0.4258

1.118181	20	OACOxford	-0.4166	0.3896	-0.3985	-0.6252	0.4665	-0.2912	-0.8287	-0.4840	-1.2471	-1.1116	-0.4466	-0.3704
1.278577	20	Roland	-0.6444	-0.2199	-0.6811	-0.9509	1.1145	-0.6182	-1.2871	-1.2012	-1.1826	-1.0719	0.1210	-1.1695
1.377195	20	OAC7-23C	-0.6243	0.3896	-0.6652	-0.9509	0.1066	-0.2912	-0.1985	-1.1360	-0.6026	-0.6353	-0.5034	-1.0649
1.526821	20	OT11-09	-0.5451	0.7378	-0.6027	-0.6252	0.6321	-1.5993	-1.9746	-0.9404	-1.6982	-1.4973	-0.7304	-0.8004
2.150815	20	Stratfor	-0.5037	0.1719	-0.5449	-0.6252	1.7121	-0.4220	-0.1985	-0.7448	-0.4737	-0.5502	0.7453	-0.7191
2.163745	20	ACOrford	-0.6377	1.0860	-0.6969	-0.9509	-0.9302	-1.4031	-0.3704	-1.1360	-0.0870	-0.1135	0.3480	-1.0707
1.081495	21	S14-P6	-0.3396	1.0860	-0.3043	-0.2995	1.2081	-0.0950	-0.7715	-0.0928	0.8152	0.9073	-0.3331	-0.0769
1.282782	21	Walton	-0.4926	0.8684	-0.4439	-0.6252	2.0216	-1.1742	-0.7142	-0.6796	0.8152	0.8960	-1.2412	-0.6813
1.438648	21	S12-A5	-0.4055	2.2614	-0.4370	-0.2995	1.2081	-0.6182	-0.7142	-0.4188	-0.3448	-0.3063	-0.7304	-0.3413
1.27531	22	McCall	-0.3463	1.3472	-0.3190	-0.2995	0.0778	-0.5201	2.6089	-0.1580	1.3953	1.3497	0.5183	-0.1495
1.306172	22	OACLakeview	-0.3295	0.3460	-0.2759	-0.2995	0.4665	-0.0950	2.0360	-0.0276	0.5575	0.5444	-0.5034	-0.0478
1.605831	22	Proteus	-0.0091	-0.2634	-0.0262	0.3518	1.0425	0.1339	2.2842	0.4288	2.0398	2.1153	0.0642	0.5363
2.579318	22	OACKent	-0.5663	-0.4811	-0.5834	-0.9509	0.3946	1.3439	2.0360	-1.0056	0.9441	1.1058	0.2913	-0.8440
1.449025	23	5091_50j	-0.1230	-0.0893	-0.1465	0.3518	-1.2397	-0.6182	-0.7142	0.3636	-0.5382	-0.5956	-0.4466	0.4898
1.505267	23	Gentleman	-0.3619	1.3472	-0.3689	-0.2995	-0.4478	0.0358	-0.3322	-0.2232	0.1708	0.0963	0.4048	-0.2076
1.509005	23	4067P17j	-0.2480	0.6507	-0.2441	0.0262	-1.6717	0.7880	-0.1412	0.1680	-0.2159	-0.1929	0.6318	0.3067
1.514055	23	Evans	0.0222	1.1731	-0.0319	0.3518	-0.4982	-0.1931	0.3744	0.4940	-0.0226	-0.0568	0.8588	0.6060

1.590677	23	ACProtei	0.0166	0.7813	-0.0273	0.3518	-0.8582	-0.3566	0.1262	0.4288	-1.2471	-1.1627	1.1994	0.5624
1.591632	23	4042_6Bp	-0.2849	1.1296	-0.2940	0.0262	-1.7941	-0.4220	-0.1985	0.1028	0.1063	0.0510	0.8588	0.1469
1.612227	23	Carman	-0.3776	0.9555	-0.3746	-0.2995	-0.6638	-0.9453	-1.1534	-0.2884	-0.3448	-0.3347	0.5183	-0.2541
1.690578	23	90A01	0.0200	0.0413	-0.0035	0.3518	-1.0453	0.5591	0.3744	0.4940	-1.1182	-0.9245	-0.5601	0.6002
1.711989	23	91M10	-0.4200	-0.6552	-0.3315	-0.6252	-0.9518	-0.0950	0.2407	-0.5492	-0.7315	-0.6409	0.8588	-0.3820
1.741604	23	9063	-0.4959	1.0860	-0.5608	-0.6252	-1.1461	-1.0761	-0.3895	-0.6796	-0.4737	-0.4991	-0.1061	-0.7045
1.74669	23	Brant	-0.4602	1.1731	-0.4189	-0.6252	-0.7574	0.2320	0.0498	-0.6144	0.1708	0.0963	0.5750	-0.5970
1.091571	24	Flambeau	-0.5618	-0.9599	-0.5664	-0.6252	-0.4694	1.0169	0.1262	-1.0056	-0.3448	-0.2723	0.0642	-0.8121
1.097031	24	Drayton	-0.3496	-0.9599	-0.2963	-0.2995	-0.4982	1.1150	-0.0075	-0.1580	-0.0226	-0.0341	-0.1061	-0.2047
1.266823	24	Elora	-0.3742	-0.4811	-0.3326	-0.2995	-0.4982	0.5591	0.1262	-0.2232	-0.3448	-0.3007	0.8588	-0.2396
1.284333	24	OAC7-48C	-0.4836	-1.3517	-0.3758	-0.6252	0.1498	0.3628	-0.2558	-0.6796	0.4930	0.4309	-0.4466	-0.6726
1.354878	24	OACMorris	-0.5149	0.2154	-0.5573	-0.6252	0.4665	1.2131	0.5081	-0.7448	0.0419	0.0113	0.2913	-0.7249
1.379223	24	Krios	-0.3295	0.0413	-0.2668	-0.2995	-0.1814	1.1150	0.1835	-0.0928	0.6219	0.6124	-0.2196	-0.0478
1.49045	24	OT10-02	-0.4647	0.0848	-0.3939	-0.6252	0.5385	0.2320	-0.3895	-0.6796	0.4930	0.5217	0.6318	-0.6203
1.648873	24	5030_46B	-0.3150	-0.2634	-0.2430	-0.2995	-1.4341	0.7226	0.3744	-0.0276	-0.2804	-0.2042	-0.6169	-0.0391
1.70438	24	Jutra	-0.6724	-1.3517	-0.6799	-0.9509	-0.3254	-0.0950	0.0498	-1.3316	-0.1515	-0.1645	0.4048	-1.3206
1.919037	24	Altesse	-0.6422	-1.4387	-0.6357	-0.9509	-0.7862	0.1339	-0.7142	-1.1360	-0.4093	-0.4595	-0.4466	-1.1433

1.924057	24	MapleBelle	-0.5227	-0.1763	-0.5562	-0.6252	-0.1382	1.2131	1.5203	-0.7448	0.7508	0.7485	0.4048	-0.7394
2.02974	24	SECAN8-1	-0.3496	-0.8293	-0.2986	-0.2995	1.4457	0.1339	0.0498	-0.1580	-0.4093	-0.4651	-0.3331	-0.1844
2.367129	24	Dares	-0.1274	-0.5246	-0.1397	0.0262	-0.5414	0.0358	1.5776	0.2984	0.0419	-0.0228	-1.0710	0.4869
2.525529	24	4043P2j	-0.6679	0.4331	-0.7230	-0.9509	-1.7437	0.0358	-0.3895	-1.2012	-0.6026	-0.6069	-1.0142	-1.2247
0	25	OAC7-6C	-0.8265	-1.3952	-0.8206	-1.6023	0.1498	-1.5012	-1.4781	-1.7880	-1.3115	-1.2364	-5.8955	-1.8349
0.954529	26	OACWalla	0.0635	-0.7858	0.0601	0.6775	0.4881	-0.0950	0.1835	0.7548	1.7820	1.9054	0.3480	0.6525
1.211037	26	MapleGlen	0.3025	0.3460	0.2723	0.6775	-0.0662	0.7880	0.3171	0.8852	1.3308	1.3383	0.2913	0.8472
1.297784	26	DH420	0.6029	-0.9164	0.6116	1.0032	-0.5918	0.3628	-0.1985	1.2112	2.4264	2.3365	-0.3331	1.1116
1.786338	26	Ginty	-0.1721	-0.0458	-0.1976	0.0262	-0.4262	0.4609	-0.1412	0.2984	1.3308	1.2759	-0.6169	0.4404
0	27	S03-W4	-0.1676	0.5201	-0.2078	0.0262	1.1361	-1.1742	-0.6378	0.2984	0.3641	0.3799	-4.7035	0.4723
0	28	Venus	2.0903	2.2178	2.0201	1.9803	1.8057	0.2320	1.2720	1.7980	-1.3115	-1.3101	0.0075	1.6463
0.844357	29	Gaillard	-0.0649	0.9990	-0.1147	0.3518	-0.4694	2.6520	1.5776	0.3636	-0.0226	-0.0511	-0.7872	0.5246
1.153577	29	Auriga	-0.2547	1.2602	-0.2679	0.0262	-0.7574	2.0961	2.1506	0.1680	-0.4093	-0.3687	0.5183	0.2195
1.374628	29	Mario	0.1897	1.0860	0.1395	0.6775	0.0346	2.7501	1.5776	0.8200	0.1063	0.0510	-0.1628	0.7775
0.998249	30	OAC7-4C	0.8519	0.5201	0.8057	1.0032	0.1498	-0.4220	-0.1985	1.3416	0.1063	0.0113	-0.2763	1.3499
1.081087	30	PRO25-53	1.6481	0.4766	1.6160	1.3289	0.6537	0.3628	0.3171	1.6024	0.4930	0.4536	0.2345	1.5969
1.142876	30	Mandarin	0.9189	0.8684	0.8658	1.3289	-0.1382	0.2320	-0.2558	1.4720	0.6863	0.7428	-0.2196	1.4371

1.257739	30	OACPrudence	1.2573	-0.1328	1.2358	1.3289	0.4881	-0.6182	-1.0961	1.6024	0.6863	0.7031	-0.2196	1.5446
1.55522	30	Kamichis	1.2014	-0.9164	1.1984	1.3289	-0.2102	0.1339	-0.1412	1.4720	0.8797	1.0661	0.2345	1.4603
1.607012	30	MapleDonovan	0.7101	-0.0022	0.6956	1.0032	-0.1094	0.5591	0.8710	1.3416	0.6219	0.6181	-0.2763	1.2802
1.755262	30	Toki	0.6420	0.0413	0.6264	1.0032	1.7841	-0.6182	-0.7142	1.2764	0.4286	0.3856	0.3480	1.2221
1.882818	30	Saska	2.0713	-0.0458	2.0598	1.6546	1.5897	-0.1931	0.1262	1.6676	0.4930	0.4196	-0.1061	1.6434
2.167402	30	MaplePresto	0.5057	1.1731	0.4584	1.0032	-0.0158	-0.6182	0.4317	1.0808	-0.4093	-0.3801	-0.5601	1.1000
2.451485	30	SECAN8-2	0.8999	0.6072	0.8522	1.0032	1.4745	-0.5201	-0.0075	1.4068	-0.9893	-0.9188	0.8021	1.4255
2.482569	30	5085_8Bp	1.2483	0.9990	1.1972	1.3289	-1.3333	-0.9453	-0.0075	1.5372	1.2664	1.2703	0.9156	1.5039

Table B 2: Numerical information presented in supplement to that in Table 3.1 (right half)

Cluster analysis applied to the first six principal components from the preliminary PCA performed on the dataset for the 12 RSA-related traits after standardized, including the distance to the centroid and the *Prin1-Prin6* scores for each of the 137 soybean lines. White and yellow colours are used to highlight lines that are members of different clusters from Cluster 1 to Cluster 30, while red is used to identify clusters with only one member**.**

Distance	Cluster	Line	*Prin1*	*Prin2*	*Prin3*	*Prin4*	*Prin5*	*Prin6*
1.330548	1	4004P4J	-0.20656	-0.15432	-2.04757	-1.67709	0.729894	-1.7157
1.392867	1	5017_25B	-0.959	-1.45933	-1.76732	-1.12985	0.965888	-0.0868
1.436877	1	Bloomfield	-0.07392	-0.33199	-0.59798	-0.86269	-0.59623	-0.6398
0	2	4005_24j	1.770632	-1.68441	-1.91051	-0.19973	-0.53428	-3.00415
0.903904	3	PS44	1.654187	-0.72875	-2.17273	1.57129	0.758509	0.345872
0.964755	3	OAC9-48C	0.942252	-0.69559	-1.64217	1.770093	0.431012	-0.17159
1.251096	3	SECAN9-3	1.862934	-1.39112	-0.77204	1.812982	0.172326	0.751896
1.34092	3	Phoenix	2.931238	-0.71081	-1.87471	2.256634	0.712191	-0.19064
1.488738	3	Hercule	1.914302	-0.97251	-1.06208	0.772799	0.040392	-1.13871
1.124655	4	OAC7-26C	6.7597	-2.06606	1.649882	0.286508	0.972291	-0.28298
1.124655	4	OACBayfield	6.82274	-1.88194	3.47351	-0.88718	0.548711	0.08972

1.020093	5	Gretna	-2.16439	0.630564	0.07599	0.345438	0.186796	-0.20604
1.090915	5	OAC7-23C	-2.0634	-0.42744	-0.18394	0.837152	-0.0877	0.231784
1.097175	5	MapleIsle	-1.8243	-0.2931	0.738313	0.460852	0.483973	0.203445
1.198203	5	AC2001	-1.4314	-0.05938	0.691225	-0.54135	0.739782	-0.4879
1.341361	5	9063	-1.50845	-0.98326	-0.71424	0.455144	1.173753	-0.41458
1.400791	5	4043P2j	-2.49156	-0.70061	-0.29292	0.306708	0.343006	-1.4895
1.49227	5	91M10	-1.53114	-0.01207	0.399357	-1.09618	0.562365	0.025838
1.578476	5	Flambeau	-1.84004	0.587904	0.277908	-0.71493	-0.59813	-0.30498
1.712594	5	ACOrford	-1.80092	-0.81489	-1.43354	0.250367	1.019184	0.127051
1.748471	5	Heather	-1.33331	0.953854	0.672347	0.976158	0.155887	-0.91943
1.997445	5	OT11-02	-1.34319	0.512374	0.141019	1.230973	1.083498	0.817481
0.844417	6	Madoc	-3.27298	0.365985	0.817858	-0.31146	-0.16569	0.602869
1.273004	6	Colby	-3.54467	-0.34459	1.296343	-0.00344	-1.26405	-0.6403
1.314424	6	Altona	-3.50214	-0.6549	1.313351	-0.63567	-1.05128	-0.26649
1.489835	6	Casino	-4.3733	0.470132	0.960399	1.06709	-0.14135	-0.4645
1.924092	6	Amasa	-3.29733	1.37474	1.033897	-0.62224	1.030084	0.415849

1.121011	7	OACPrudence	3.286357	-1.1774	0.047875	-0.20711	-0.08967	0.045533
1.390005	7	Saska	4.128291	-0.21712	1.317002	0.276166	-0.352	0.807936
1.500751	7	MapleArrow	4.470498	-2.06206	1.262645	-1.34669	0.266108	0.0513
0.944889	8	OACWallace	1.979215	0.758553	-1.48555	-0.90498	-1.18758	0.104095
1.369858	8	OT11-03	1.907641	-0.25256	-0.73211	-1.2991	-0.72994	0.744836
1.477678	8	Katrina	1.394601	0.651079	-0.55116	-0.66183	0.195316	-0.19687
1.524441	8	DH420	3.002459	0.525476	-1.58467	-1.3401	-1.32931	-1.33768
1.69266	8	Kamichis	3.090677	-0.04358	0.270452	-1.28362	-0.35887	-0.48238
1.239143	9	5055_43G	-2.11929	-0.31204	2.389781	0.88467	-0.33172	-2.4206
1.239143	9	90A07	-2.34637	1.781666	2.380786	-0.00465	-0.14879	-1.48129
1.10524	10	Costaud	1.066894	-0.711	0.213361	-0.44821	-0.29761	-0.87539
1.366054	10	KG-41	-0.00345	-0.3005	1.694259	0.02242	-0.8619	-1.24762
1.397004	10	DH618	0.005746	-0.81758	0.938972	0.329501	-0.25406	-1.00099
1.410547	10	5070_26j	0.894363	-1.32447	1.261415	-2.07979	-0.71783	-1.33707
0.929683	11	Mandarin	2.87362	0.017451	-0.06222	0.284094	0.630874	-0.76464
0.929683	11	5085_8Bp	3.406451	-0.21081	-0.92999	-0.93938	1.563431	-0.80522

1.989973	11	MapleDonovan	2.319144	0.829031	0.497107	-0.10366	-0.08078	-0.85576
0	12	Venus	3.504441	0.443113	3.07661	2.264172	1.865961	0.992531
0	13	OAC7-6C	-3.51238	-3.94506	0.694758	2.791207	-3.81182	-1.94384
1.025438	14	MapleGlen	1.950515	1.212767	-0.87818	-0.29554	-0.05199	-0.57655
1.133581	14	Misty	0.957905	1.125098	-1.93175	0.473249	-0.33819	-0.6243
1.376547	14	Proteus	1.862329	2.421973	-1.29305	-0.01608	-1.58936	0.147437
1.554006	14	Ginty	0.825602	0.481711	-1.31164	-0.13592	-0.74981	-1.10093
1.561721	14	OACChampion	0.803258	0.570236	-1.82936	-0.28124	-0.47042	0.300974
1.111696	15	Bravor	1.286329	-2.17981	-0.94501	-0.84149	0.940364	0.100996
1.149608	15	MapleRidge	0.16274	-1.0078	-0.64594	0.215294	0.378599	0.086198
1.403277	15	OAC9-22C	0.392876	-1.3315	-1.21992	0.127763	-0.42205	0.238089
1.568972	15	Naya	1.448332	-0.66196	-1.08196	-0.65097	0.511245	0.759397
1.907814	15	90B11	-0.85748	-2.8683	-0.50978	-1.08654	0.303269	0.071198
2.06738	15	5146_41j	0.804575	-1.97405	1.088615	-1.53843	1.158925	-0.17975
0	16	Tundra	2.392434	-0.00919	-3.11959	0.165908	-2.23717	0.720008
1.026367	17	SECAN8-1	-2.82205	1.656586	1.940391	0.237208	-1.0961	1.254622

1.035492	17	OAC1-26	-2.06458	0.71528	1.119125	-0.44278	-0.12782	0.755036
1.50557	17	OAC9-35C	-2.24928	1.980036	0.392426	0.583123	0.026494	0.28567
2.170144	17	OAC7-3C	-2.02314	3.050042	1.847766	-0.2462	-0.55075	-0.29354
2.555418	17	Victoria	-2.94044	-0.50777	1.515473	0.249691	-0.86856	2.487679
0	18	Woodstock	9.434811	1.821216	2.576142	0.148041	-2.45656	2.60001
0.775305	19	Jutra	-2.25111	0.019309	-0.27515	-1.10176	-0.86656	0.401377
1.241702	19	Dundas	-3.03428	0.057752	-0.82016	-2.42551	-0.91257	1.23992
1.249249	19	Albinos	-3.00033	-0.94026	-0.37114	-1.98963	-1.63841	0.19325
1.345855	19	OAC9-17C	-1.7492	-0.5939	-0.66762	-0.7842	-0.24144	0.999309
1.486543	19	Altesse	-2.3293	-0.75828	0.003871	-0.89567	-0.9591	-0.41837
0.728379	20	OT94-47	7.153823	-0.95995	0.814329	-1.47658	-1.23569	0.056048
0.728379	20	OAC8-21C	6.152977	-1.13569	0.116077	-1.04452	-0.65484	-0.22312
0.651441	21	Alta	-2.35283	-0.78953	-0.05158	-0.87575	0.539341	0.475198
0.991284	21	DH530	-2.391	-0.8336	0.151482	-0.22234	1.057945	0.594303
1.351991	21	Clinton	-1.84107	-0.97596	0.685349	-0.57948	0.181966	0.008464
1.418812	21	9004	-3.90855	-1.3628	0.397868	-0.96748	0.360247	0.33015

1.460741	21	ACGlengarry	-3.62941	-2.08626	0.507335	-1.30224	0.226576	0.849288
1.664939	21	4028P7j	-3.1541	-0.97794	1.043664	-1.32752	1.585948	0.020585
1.701912	21	Madison	-1.88605	-1.2658	-1.2704	-0.54916	0.438511	1.191067
2.058549	21	OAC8-22C	-0.87265	-1.78016	0.123878	-1.40592	0.241705	1.52625
1.090354	22	McCall	0.475332	2.283749	-1.54313	0.617624	0.181623	0.036456
1.371486	22	SECAN7-2	0.94133	1.734751	-1.62682	0.013336	1.001819	1.648522
1.374978	22	Jari	0.42858	2.092761	-1.22674	0.615443	1.582439	-0.10791
1.46743	22	Ohgata	0.391732	1.576233	-0.18138	0.728714	-0.07183	0.077655
1.916493	22	SECAN8-1	0.190037	1.766774	-0.0326	1.395136	0.323586	0.893865
1.924913	22	KORADA	0.796046	0.138305	-2.16059	-0.71115	0.748024	0.503303
2.183383	22	OACAyton	0.239793	3.639512	-0.91773	-0.30924	1.03602	0.492437
1.107881	23	4067P17j	-0.35706	0.419181	-0.10133	-0.60456	1.522713	-1.18046
1.352671	23	Gentleman	-0.44099	0.189333	-0.96034	0.480739	1.112223	-0.14512
1.400772	23	4042_6Bp	-0.208	-0.13436	-0.91994	-0.5139	1.894501	-0.85746
1.42335	23	Evans	0.610755	0.41395	-0.22497	0.11068	1.564922	-0.06937
1.456422	23	Brant	-1.02616	0.581807	-0.95137	0.176985	1.040441	-0.2483

1.476966	23	ACProteina	-0.19762	-0.28835	0.941623	-0.26989	2.229461	0.135455
1.506418	23	5091_50j	-0.10773	-1.35208	0.286443	-0.27505	0.703671	-0.99715
1.614032	23	Carman	-0.77737	-1.16541	-0.86105	0.110712	1.347852	0.188331
1.695816	23	90A01	-0.20019	-0.1248	1.456272	0.107134	0.76088	-1.25805
1.714167	23	5030_46B	-0.80477	0.269737	0.3752	-0.34397	0.082361	-1.58965
0	24	S03-W4	0.701144	-2.11331	-0.40465	3.411648	-2.53768	-1.61214
0.975369	25	Roland	-2.32112	-1.28779	0.111746	0.56415	-0.20373	1.62888
1.059605	25	OACOxford	-1.4738	-1.0613	0.539552	0.99529	0.337259	0.50819
1.270806	25	OT09-03	-2.08124	-1.86289	1.097987	0.184749	-0.90676	0.731327
1.41349	25	OT11-09	-2.05585	-2.73331	0.140375	1.497938	0.596295	1.056014
1.429122	25	Purdy	-1.05801	-1.01881	0.540989	0.119985	-0.42711	1.190377
1.578908	25	OT11-01	-1.52352	-1.47635	-0.31697	-0.16788	-0.83495	0.888424
1.015101	26	MapleBelle	-0.95299	2.235698	-0.60345	-0.36073	-0.65182	-0.26621
1.039663	26	OACKent	-1.05662	2.771455	-0.68902	-0.26498	-1.3645	0.020862
1.821556	26	Delta	0.303821	3.615807	-0.21025	-2.33322	-0.74948	-0.54365
1.968453	26	PS36	-1.1232	2.320863	-0.30653	0.214177	-0.0081	0.710073

0.812049	27	OAC7-4C	2.272425	-0.59879	0.507522	0.389385	0.576357	-0.24987
1.395186	27	MaplePresto	1.586797	-0.4355	0.734765	1.109277	1.026007	-0.44825
1.465076	27	Toki	2.471991	-0.55593	-0.01277	0.371975	-0.18009	1.378587
1.479554	27	PRO25-53	3.493394	0.404747	0.932426	0.10011	0.424079	0.095749
1.524081	27	SECAN8-2	1.997174	-0.44931	1.592664	0.663056	1.201516	1.502396
1.002491	28	S14-P6	0.366651	0.053917	-1.57329	1.268256	-0.36551	0.61092
1.224986	28	Walton	-0.18636	-0.71032	-1.81004	2.044111	-1.41811	1.160473
1.432934	28	S12-A5	-0.49183	-0.6201	-0.78764	2.549722	0.707164	0.732004
0.924578	29	Mario	1.025956	2.75571	1.076591	0.858192	0.535622	-1.19659
1.152542	29	Gaillard	0.260606	2.470455	0.988941	1.000909	0.292871	-1.79438
1.643582	29	Auriga	-0.39575	2.785033	0.956169	0.476558	1.326183	-1.06425
1.209572	30	OT05-20	-0.13876	-0.31209	-0.28224	-0.01688	0.184863	0.822197
1.242202	30	OAC9-44C	-0.9444	0.715403	0.627507	0.176825	0.639816	0.109285
1.25876	30	Lotus	-0.31278	0.448477	0.955385	0.134457	0.049093	-0.58529
1.277664	30	OACMorris	-1.23343	1.407253	-0.16387	0.310295	-0.25968	0.29335
1.304901	30	SECAN8-1	-0.62958	0.001721	0.61987	0.442547	-1.121	0.988649

1.340199	30	Drayton	-0.7802	0.535816	0.28064	-0.74783	-0.59344	-0.65564
1.34577	30	Elora	-0.93223	0.512442	0.225457	-0.88579	0.372077	0.058868
1.349564	30	Krios	-0.14737	1.03599	-0.56197	-0.00327	-0.44704	-0.67298
1.376278	30	OT10-02	-0.73834	0.478623	-1.09659	-0.11302	-0.28274	0.781664
1.459258	30	MapleAmbr	0.577359	-0.2273	-0.26634	-0.14262	-0.18475	-0.31502
1.506564	30	OACLakeview	0.047398	1.480173	-0.2673	0.822498	-0.67953	-0.16291
1.658561	30	S05-T6	0.906997	0.536344	-0.20045	0.562478	0.078445	0.863491
1.709452	30	Dares	0.089725	0.599769	0.655969	0.157708	-0.69857	-1.21514
1.711745	30	OAC8-11C	-0.78862	0.486544	-0.63292	1.385123	0.051295	-0.4716
1.747889	30	OAC7-48C	-0.9968	0.07935	-0.48931	-0.61869	-1.60996	-0.0756
2.027466	30	Perth	-0.3454	0.439457	1.598644	1.439207	-0.00559	-0.03862
2.101681	30	Stratford	-1.23741	0.015423	-0.13725	0.664496	-0.11212	2.059081
2.293443	30	SECAN7-4	0.912087	1.319651	0.220788	-1.02794	-1.03815	1.112695
2.591547	30	Supra	1.26182	1.643742	1.186795	-0.22983	-0.90362	1.081433

Appendix C: Supplementary Figure

Figure C1: Skeletal 3D images of root systems, as reconstructed from CT scanning data, for 30 soybean cultivars (n = 2, 3, or 4), with the corresponding FD estimates.

Cultivar	POT1	POT2	POT3	POT4
4004P4J	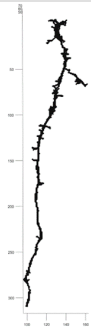 FD = 1.3983	 FD = 1.214	 FD = 1.0954	 FD = 1.4416
400524J	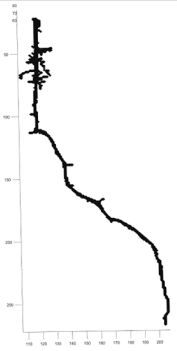 FD = 1.3326	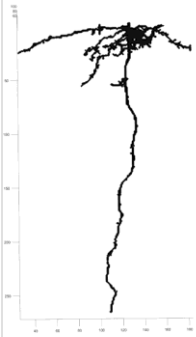 FD = 1.5989	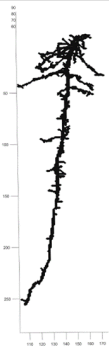 FD = 1.5989	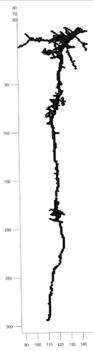 FD = 1.4534
PS44	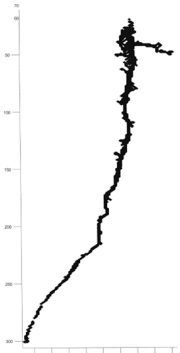 FD = 1.219	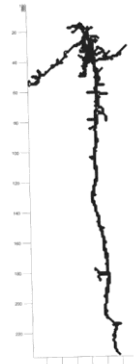 FD = 1.459	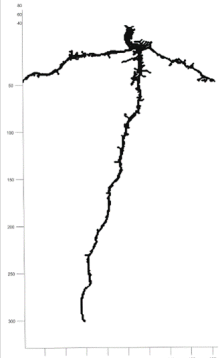 FD = 1.3443	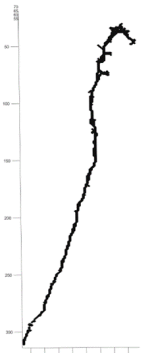 FD = 1.2506
OAC726-C	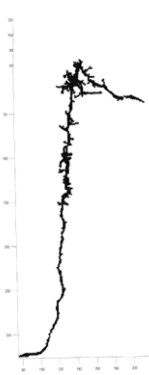 FD = 1.3848	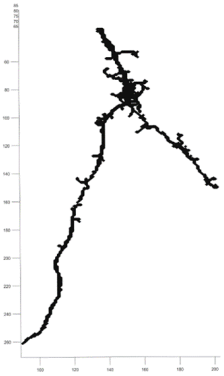 FD = 1.1684	 FD = 1.3136	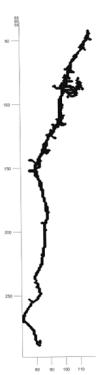 FD = 1.2506

Cultivar	POT1	POT2	POT3	POT4
AC2001	 FD = 1.3581	 FD = 1.3757	 FD = 1.3486	 FD = 1.4149
CASINO	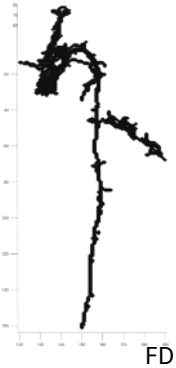 FD = 1.4871	 FD = 1.2114	 FD = 1.223	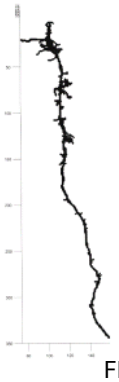 FD = 1.4149
SASKA			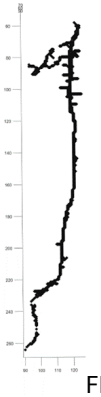 FD = 1.2773	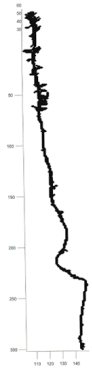 FD = 1.2896
OAC-WALLACE	 FD = 1.4414	 FD = 1.39	 FD = 1.4501	

Cultivar	POT1	POT2	POT3	POT4
505543G		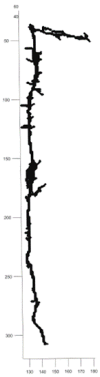 FD = 1.4975	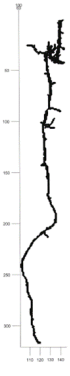 FD = 1.3161	 FD = 1.3194
COSTAUD	 FD = 1.4175	 FD = 1.4313	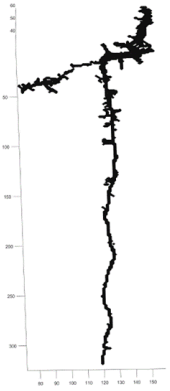 FD = 1.3211	
MAPLE DONOVAN	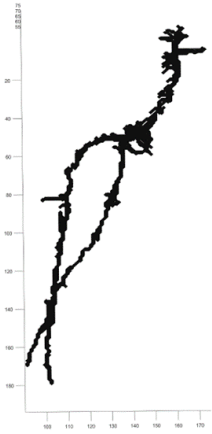 FD = 1.4334	 FD = 1.3808	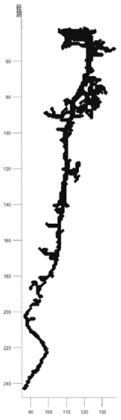 FD = 1.5286	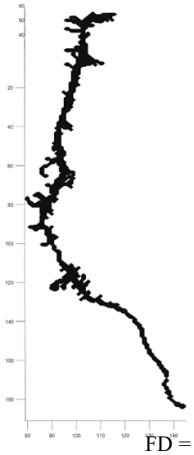 FD = 1.4431
VENUS	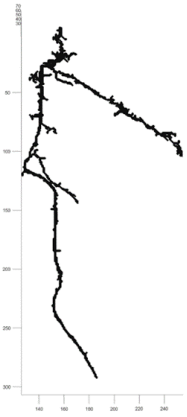 FD = 1.4095	 FD = 1.3869	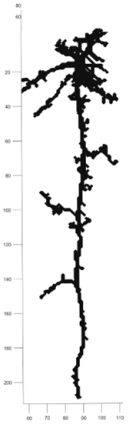 FD = 1.5939	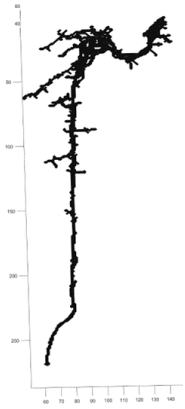 FD = 1.6538

Cultivar	POT1	POT2	POT3	POT4
OAC7-26C	 FD = 1.3274	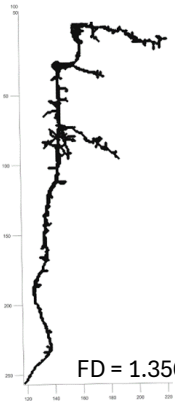 FD = 1.3562	 FD = 1.3388	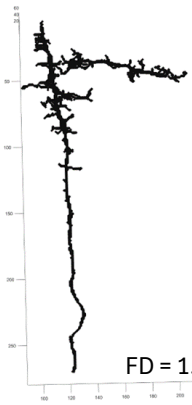 FD = 1.4682
OAC-CHAMPION	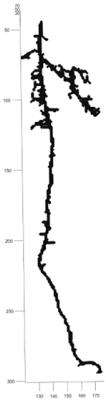 FD = 1.3699	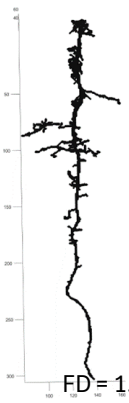 FD = 1.372	 FD = 1.3937	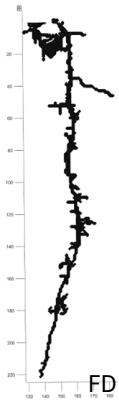 FD = 1.4371
OAC9-22C	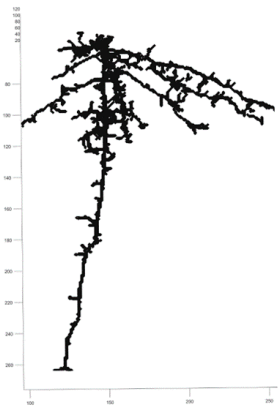 FD = 1.6078	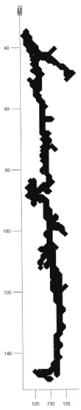 FD = 1.5153	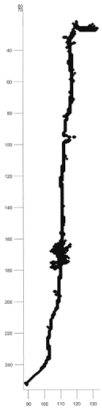 FD = 1.3148	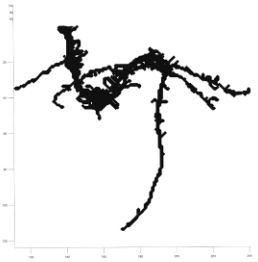 FD = 1.4687
TUNDRA	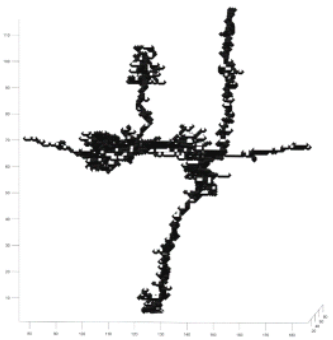 FD = 1.5706	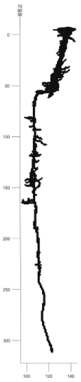 FD = 1.3191		

Note: TUNDRA (POT1) is shown from the top to make lateral roots more visible.

Cultivar	POT1	POT2	POT3	POT4
OAC1-26C	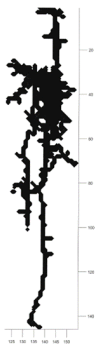 FD = 1.6108	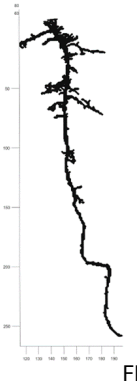 FD = 1.4728	 FD = 1.4725	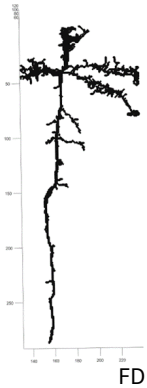 FD = 1.6143
WOODSTOCK	 FD = 1.2575	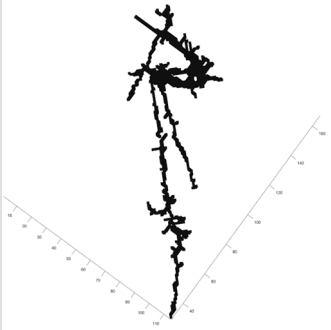 FD = 1.5329	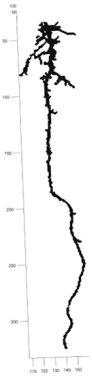 FD = 1.3863	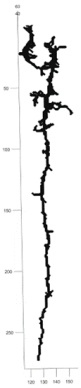 FD = 1.4443
DUNDAS	 FD = 1.408	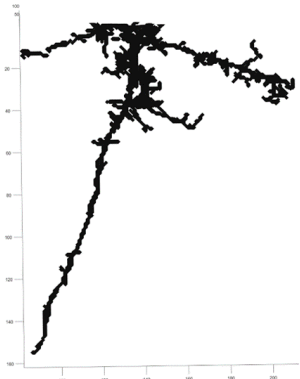 FD = 1.5117	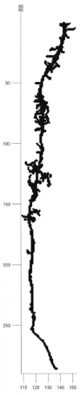 FD = 1.4774	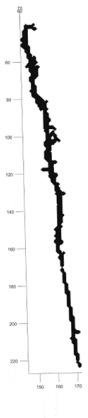 FD = 1.3894
OAC8-21C	 FD = 1.4295	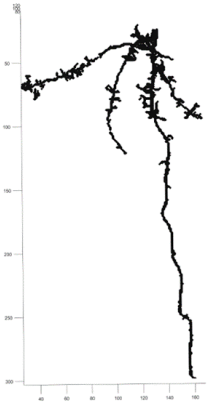 FD = 1.4535	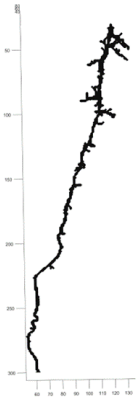 FD = 1.3414	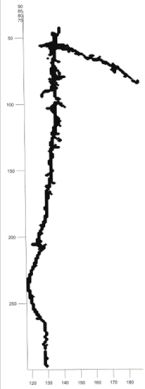 FD = 1.3662

Cultivar	POT1	POT2	POT3	POT4
ACGLENGARRY	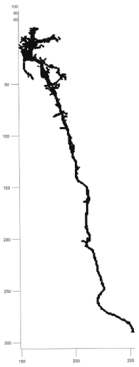 FD = 1.3764	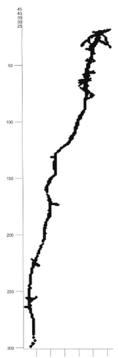 FD = 1.3473	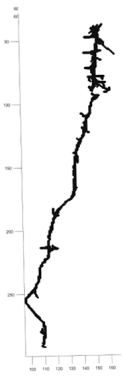 FD = 1.3188	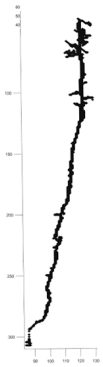 FD = 1.3141
McCALL			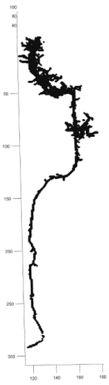 FD = 1.5308	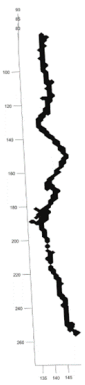 FD = 1.2812
GENTLEMAN	 FD = 1.3324	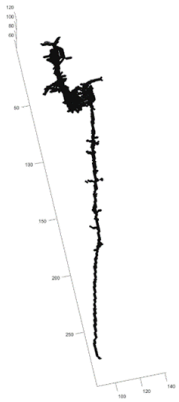 FD = 1.4226	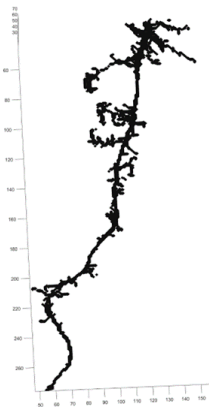 FD = 1.5002	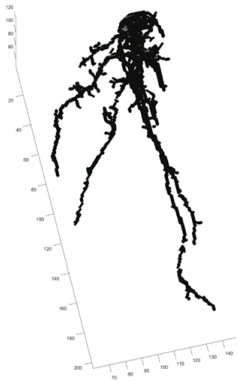 FD = 1.546
S03-W4	 FD = 1.6163	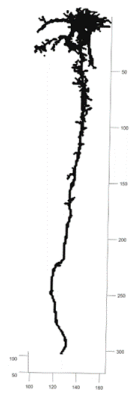 FD = 1.5896	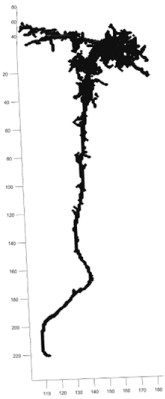 FD = 1.574	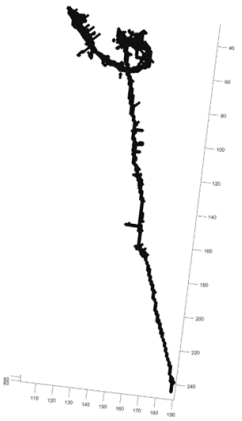 FD = 1.3381

Cultivar	POT1	POT2	POT3	POT4
OAC-OXFORD	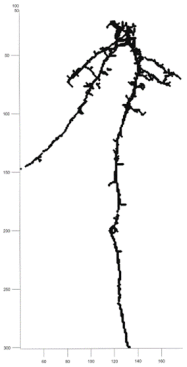 FD = 1.4892	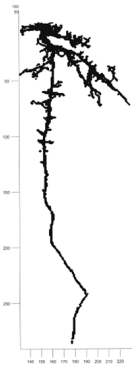 FD = 1.4686	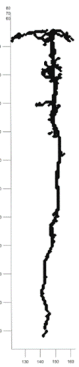 FD = 1.3587	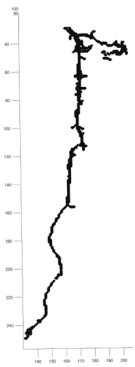 FD = 1.3502
OAC-KENT	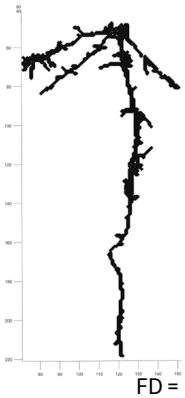 FD = 1.5415	 FD = 1.3677	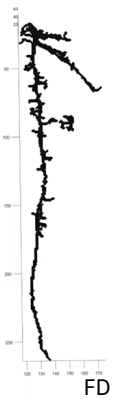 FD = 1.5462	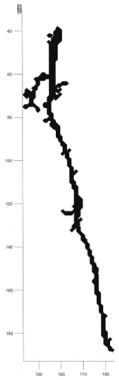 FD = 1.1957
OAC7-4C		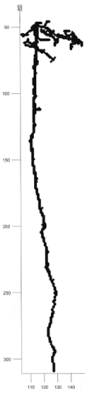 FD = 1.3412	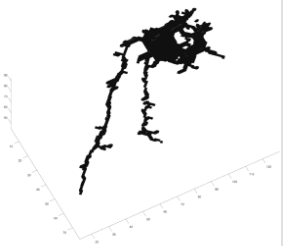 FD = 1.5543	 FD = 1.2613
WALTON	 FD = 1.263	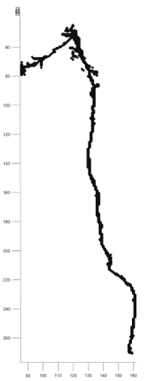 FD = 1.2914	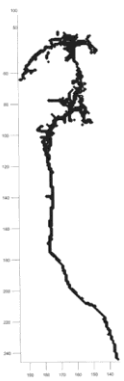 FD = 1.3188	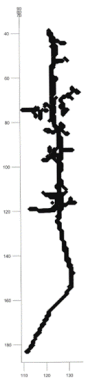 FD = 1.4327

Cultivar	POT1	POT2	POT3	POT4
GAILLARD	 FD = 1.4177	 FD = 1.4129	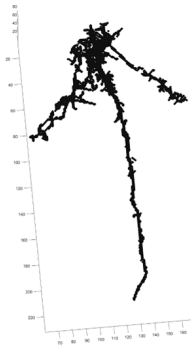 FD = 1.462	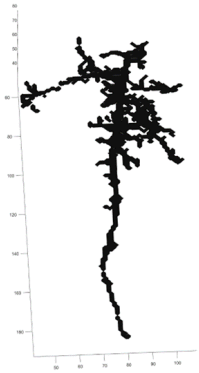 FD = 1.5187
DRAYTON	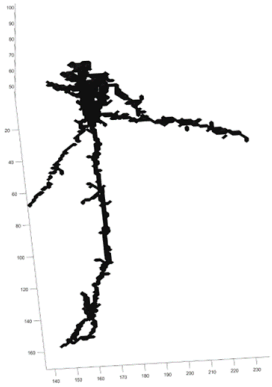 FD = 1.5193	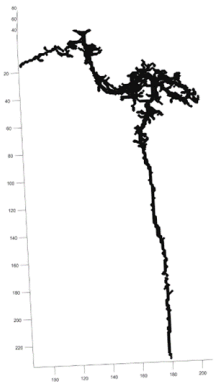 FD = 1.4996	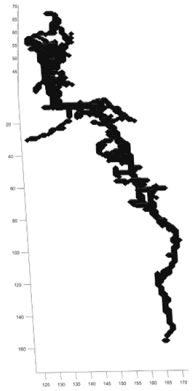 FD = 1.3497	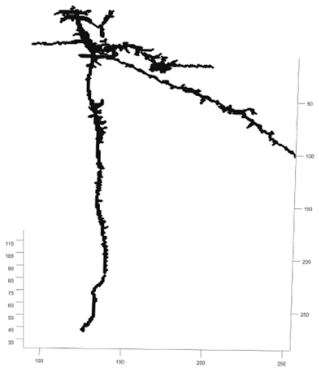 FD = 1.3828

Appendix D: Supplementary Table

Table D1: Summary of statistically significant ($p < 0.05$) pairwise comparisons between cultivars based on FD means

Cultivars	Difference between FD Means	95% Confidence Limits	
17-20	0.14495	0.00464	0.28526
17-14	0.14942	0.00911	0.28974
17-11	0.15263	0.00108	0.30419
17-27	0.157	0.00545	0.30855
17-9	0.16493	0.01338	0.31649
17-5	0.16827	0.02796	0.30859
17-13	0.16995	0.02964	0.31026
17-21	0.20345	0.06314	0.34376
17-28	0.21612	0.07581	0.35644
17-3	0.22438	0.08406	0.36469
17-6	0.24018	0.09986	0.38049
17-4	0.24392	0.10361	0.38424
17-1	0.25527	0.11496	0.39559
17-7	0.25915	0.08731	0.43099
24-9	0.15183	0.00028	0.30339
24-5	0.15517	0.01486	0.29549
24-13	0.15685	0.01654	0.29716
24-21	0.19035	0.05004	0.33066
24-28	0.20302	0.06271	0.34334
24-13	0.21127	0.07096	0.35159

24-3	0.22707	0.08676	0.36739
24-5	0.23082	0.09051	0.37114
24-1	0.24217	0.10186	0.38249
24-7	0.24605	0.07421	0.41789
12-21	0.17188	0.03156	0.31219
12-28	0.18455	0.04424	0.32486
12-3	0.1928	0.05249	0.33311
12-6	0.2086	0.06829	0.34891
12-4	0.21235	0.07204	0.35266
12-1	0.2237	0.08339	0.36401
12-7	0.22757	0.05573	0.39942
2-21	0.14205	0.00174	0.28236
2-28	0.15473	0.01441	0.29504
2-3	0.16298	0.02266	0.30329
2-6	0.17878	0.03846	0.31909
2-4	0.18252	0.04221	0.32284
2-1	0.19388	0.05356	0.33419
2-7	0.19775	0.02591	0.36959
15-28	0.15017	0.00986	0.29049
15-3	0.15843	0.01811	0.29874
15-6	0.17423	0.03391	0.31454
15-4	0.17797	0.03766	0.31829
15-1	0.18932	0.04901	0.32964
15-7	0.1932	0.02136	0.36504

29-6	0.1504	0.01009	0.29071
29-4	0.15415	0.01384	0.29446
29-1	0.1655	0.02519	0.30581
23-6	0.14788	0.00756	0.28819
23-4	0.15162	0.01131	0.29194
23-1	0.16298	0.02266	0.30329
19-6	0.1442	0.00389	0.28451
19-4	0.14795	0.00764	0.28826
19-1	0.1593	0.01899	0.29961
11-6	0.14405	0.00374	0.28436
11-4	0.1478	0.00749	0.28811
11-1	0.15915	0.01884	0.29946
30-1	0.15053	0.01021	0.29084
20-17	-0.14495	-0.28526	0.00464
14-17	-0.14942	-0.28974	0.00911
10-17	-0.15263	-0.30419	0.00108
27-17	-0.157	-0.30855	0.00545
9-17	-0.16493	-0.31649	0.01338
9-24	-0.15183	-0.30339	0.00028
5-17	-0.16827	-0.30859	-0.02796
5-24	-0.15517	-0.29549	-0.01486
13-17	-0.16995	-0.31026	-0.02964
13-24	-0.15685	-0.29716	-0.01654
21-17	-0.20345	-0.34376	-0.06314

21-24	-0.19035	-0.33066	-0.05004
21-12	-0.17188	-0.31219	-0.03156
21-2	-0.14205	-0.28236	-0.00174
28-17	-0.21612	-0.35644	-0.07581
28 - 24	-0.20302	-0.34334	-0.06271
28-12	-0.18455	-0.32486	-0.04424
28-2	-0.15473	-0.29504	-0.01441
28-15	-0.15017	-0.29049	-0.00986
3-17	-0.22438	-0.36469	-0.08406
3-24	-0.21127	-0.35159	-0.07096
3-12	-0.1928	-0.33311	-0.05249
3-2	-0.16298	-0.30329	-0.02266
3-15	-0.15843	-0.29874	-0.01811
5-17	-0.24018	-0.38049	-0.09986
5-24	-0.22707	-0.36739	-0.08676
6-17	-0.2086	-0.34891	-0.06829
6-12	-0.17878	-0.31909	-0.03846
6-2	-0.17423	-0.31454	-0.03391
6-15	-0.1504	-0.29071	-0.01009
6-29	-0.14788	-0.28819	-0.00756
6-23	-0.1442	-0.28451	-0.00389
6-19	-0.14405	-0.28436	-0.00374
6-11	-0.24392	-0.38424	-0.10361
4-17	-0.23082	-0.37114	-0.09051

4-24	-0.21235	-0.35266	-0.07204
4-12	-0.18252	-0.32284	-0.04221
4-2	-0.17797	-0.31829	-0.03766
4-15	-0.15415	-0.29446	-0.01384
429	-0.15162	-0.29194	-0.01131
4-23	-0.14795	-0.28826	-0.00764
4-19	-0.1478	-0.28811	-0.00749
4-11	-0.25527	-0.39559	-0.11496
1-24	-0.24217	-0.38249	-0.10186
1-12	-0.2237	-0.36401	-0.08339
1-2	-0.19388	-0.33419	-0.05356
1-15	-0.18932	-0.32964	-0.04901
1-29	-0.1655	-0.30581	-0.02519
1-23	-0.16298	-0.30329	-0.02266
1-19	-0.1593	-0.29961	-0.01899
1-11	-0.15915	-0.29946	-0.01884
1-30	-0.15053	-0.29084	-0.01021
7-17	-0.25915	-0.43099	-0.08731
7-24	-0.24605	-0.41789	-0.07421
7-12	-0.22757	-0.39942	-0.05573
7-2	-0.19775	-0.36959	-0.02591
7-15	-0.1932	-0.36504	-0.02136